Journal of Molecular Structure 1305 (2024) 137764

Contents lists available at ScienceDirect

Journal of Molecular Structure

journal homepage: www.elsevier.com/locate/molstr

S-doped ZnO photoelectrode modified with silver and platinum nanoparticles and their photocatalytic activity for progesterone degradation

Jailson S. Luis [a,**], Samuel S. Eduardo [b], Maria J.S. Costa [a], Luciano C. Brandão-Lima [a], Renato A. Antunes [c], Raphael O. Ferreira [d], Rejane M.P. Silva [b,e], Reginaldo S. Santos [a,b,*]

[a] Department of Chemistry-PPGQ, Federal University of Piauí - UFPI, Campus Ministro Petrônio Portella, Ininga, Teresina, 64049-550, PI, Brazil
[b] Department of Chemistry-PPGQ-GREENTEC, State University of Piauí - UESPI, Campus Poeta Torquato Neto, Pirajá, Teresina, 64002-150, PI, Brazil
[c] Center for Engineering, Modeling and Applied Social Sciences - Federal University of ABC/UFABC, Bangu, Santo André, 09210-580, SP, Brazil
[d] Department of Mechatronics and Mechanical Systems Engineering - Poli/USP, Butantã, São Paulo, 05508-010, SP, Brazil
[e] Institute for Energy and Nuclear Research - IPEN/CNEN, Cidade Universitária, São Paulo, 05508-000, SP, Brazil

ARTICLE INFO

Keywords:
ZnO-S films
Doping
Metallic nanoparticles
Photoelectrochemistry
Progesterone degradation

ABSTRACT

Zinc oxide doped with sulfur (ZnO-S) has presented improved photocatalytic activity under visible irradiation. In this work, ZnO-S film was efficiently prepared by thermal decomposition from zinc sulfide (ZnS) in an oxidizing atmosphere. X-ray diffraction analysis (XRD) showed ZnS phase transformation occurred from cubic sphalerite to ZnO hexagonal wurtzite at temperatures between 500 and 600 °C. ZnO-S electrodes prepared onto a transparent conductive substrate were modified by silver (Ag^0) or platinum (Pt^0) nanoparticles (NPs). X-ray photoelectron spectroscopy (XPS) confirmed that sulfur was incorporated into ZnO structure. Field Emission Gun-Scanning Electron Microscope (FEG-SEM) images showed that occur a drastic modification in the particle morphology of the films treated at distinct temperatures. Photoelectrochemical investigation displayed a negative photopotential ($\Delta E<0$) for all photoelectrode investigated as well as superior photocurrents for samples modified with metallic Ag^0 and Pt^0 NPs. In order to investigate the photoelectroactivity, ZnO-S6, Ag^0/ZnO-S6, Pt^0/ZnO-S6 and commercial ZnO electrodes were used to degrade progesterone solution under polychromatic irradiation. The superior performances were observed for ZnO-S films functionalized with Ag^0 or Pt^0. Therefore, the results showed advances in the degradation of organic contaminants in the water treatment process and possible contributions to a better use of solar radiation.

1. Introduction

In recent years, solar energy has been considered one of the most promising sources of abundant and clean energy. Faced with the growing energy demand, intense research has been dedicated to studying materials that efficiently use solar radiation [1]. Among these materials, semiconductor oxides stand out [2]. These materials have been used for various applications, such as solar cells for conversion into electrical energy, production of fuels [3] and in Advanced Oxidative Processes (AOPs), with emphasis on heterogeneous photocatalysis (HP) and photoelectrocatalysis, showing effectiveness in degradation of organic pollutants in aqueous media [4].

The conventional effluent treatment methods generally consist of removing the pollutant by a simple phase transfer, without the occurrence of total destruction of the contaminant, requiring an extra post-treatment step. Thus, AOPs are able to transform a large part of organic contaminants into CO_2 and H_2O, in reactions with hydroxyl radicals (•OH). These radicals are not selective and can promote the destruction of a wide variety of organic pollutants in the aqueous phase, including dyes, pesticides, herbicides, and drugs such as hormones [5, 6]. Progesterone is a female sex hormone (FSH) of natural or synthetic origin, widely used as a contraceptive, and which has raised concern

* Corresponding author at: Department of Chemistry-PPGQ-GREENTEC, State University of Piauí - UESPI, Campus Poeta Torquato Neto, Pirajá, Teresina, 64002-150, PI, Brazil.
** Corresponding author.
E-mail address: rsantos.uespi@gmail.com (R.S. Santos).

https://doi.org/10.1016/j.molstruc.2024.137764
Received 7 August 2023; Received in revised form 2 February 2024; Accepted 8 February 2024
Available online 9 February 2024

when improperly disposed of in the environment [7]. Progesterone is a drug that, when discarded indiscriminately in aquatic environments, even in low concentrations (1 ng L^{-1}) can cause cancer, reduced fertility, feminization and hermaphroditism in fish and crustaceans [8]. Therefore, technological proposals for removing this pollutant from the aqueous environment deserve to be investigated.

In several countries around the world, there is already evidence of contamination of aquatic environments by female hormones, which can be classified as an emerging micropollutant due to its increasing use and imminent risk of contamination in the environment, which can cause negative impacts on fauna, flora, and harmful effects [7]. Thus, it is necessary to use advanced wastewater treatment techniques that promote the removal or destruction of these hormones.

Currently, semiconductor oxides have aroused great interest due to applications in photoelectrochemical cells (PEC), low cost, and the possibility of adjusting optical and electrical properties, to increase efficiency, stability, and use of solar radiation [9]. According to band theory, when the semiconductor absorbs photons with energy equal to or greater than its band gap energy (E_{BG}), electrons in valence band (VB) are excited to the conduction band (CB), forming the electron/hole pair (e^-/h^+) [10]. The photogenerated charges in VB and CB promote catalytic reactions that occur in the semiconductor [11].

Among the investigated semiconductors, Zinc Oxide (ZnO) has attracted attention due to its high catalytic activity, thermal stability, high charge mobility, low toxicity, and low cost [12–14]. It is an *n*-type semiconductor, with E_{BG} in the range of 3.2 to 3.4 eV [15]. This oxide can be found in hexagonal wurtzite crystalline forms (more stable) or cubic zinc blend and rock salt structures [16]. Another important semiconductor is zinc sulfide (ZnS), which is considered one of the most significant among metallic sulfides mainly due to its high stability, high quantum yield, and technological applications. For the hexagonal wurtzite phase, the ZnS has an E_{BG} of 3.77 eV, while for the cubic zinc blend phase this energy is approximately 3.72 eV [17].

Different synthesis methods have been used to obtain porous ZnO electrodes, which allow obtaining the oxide with control of morphology, particle size, and film thickness [18]. Some methods for obtaining ZnO films are described in the literature, among them we can mention the deposition from liquids as a source (sol-gel) using the spin-coating or dip-coating techniques [19], spray pyrolysis [20], chemical bath deposition [21], chemical vapor deposition [22], deposition by cathodic sputtering (*magnetron sputtering*) [23], as well as electrochemical deposition [24]. Doctor Blade deposition is also frequently used in the preparation of porous film ZnO electrodes [25–27].

Although these semiconductor oxides have several advantages and diverse applications, most of them have limitations in photocatalytic processes. For example, ZnO suffers from photocorrosion, while ZnS has a wide E_{BG} value, which limits its use in technologies using solar radiation [28]. Therefore, its applications in photocatalytic processes under visible irradiation will only be advantageous after modifying its optical properties [29]. Thus, semiconductor doping is a strategy used to gradually adjust their optical and electronic properties. However, there is a limit of doping amount to be "accommodated" into the structure. If this limit is exceeded, there may be segregation of other phases [30–32].

The insertion of metallic or non-metallic dopants in the ZnO structure can modify the absorption region to use it under visible irradiation [33]. In general, metallic sulfides such as TiS_2, when calcined in an oxidizing atmosphere, are transformed into TiO_2, because sulfur atoms can be easily replaced by oxygen. Likewise, the heat treatment of ZnS under suitable conditions leads to the formation of ZnO, with a small amount of S remaining in the material structure. In this case, the sulfur atoms can be considered a substitutional anionic dopant of ZnO [34]. Sulfur is considered a good doping because it has different oxidation states and does not generate deleterious phases in the ZnO structure [35]. Recent studies show that doping of ZnO with sulfur alters the electrical, optical, and photocatalytic properties of the semiconductor [36–37]. The doping of ZnO with substitutional S can generate energy levels above the semiconductor VB, promoting the narrowing of the E_{BG} and increasing the photocatalytic activity [38]. In order to improve the stability of the films and minimize the recombination process of the e^-/h^+ pair, another strategy is the semiconductor surface functionalization with metallic nanoparticles, which can improve the photocatalytic activity [39].

In a previous work [40], spherical microparticles generated by agglomerated spherical nanocrystals of sulfur-containing ZnO, formed by homogeneous precipitation of ZnS, were studied. In this investigation, the authors observed that the presence of Zn–S bonds in sulfur-containing zinc oxide decreases the E_{BG} value of ZnO. Despite these advances, to the best of our knowledge, the application of S-doped ZnO films in the photoelectrodegradation (or electrochemically-assisted heterogeneous photocatalysis-EHP) of progesterone, as presented in this work, has not yet been reported in the literature.

Therefore, this paper presents a simple methodology for the preparation of ZnO-S films supported on FTO-glass substrate (Fluorine Doped Tin Oxide) from pure (commercial) ZnS, which were calcined in an oxidizing atmosphere at temperatures of 100 to 600 °C, for 2 h. The films were subsequently, modified with silver and platinum nanoparticles (AgNP) and PtNP). The optical, morphological, structural, and photoelectrochemical features and their application in the degradation of progesterone in an aqueous medium under polychromatic irradiation were investigated. Thus, the present study displays advances in the degradation of organic contaminants in the water treatment process and provides contributions related to the use of solar radiation.

2. Materials and methods

2.1. ZnS suspension preparation

Initially, 1.0 g of zinc sulfide powder (ZnS - Sigma-Aldrich, 99,99 %) and 40 % by mass of polyethylene glycol (PEG 20,000 Sigma-Aldrich) were mixed and ground using an Agate mortar and pistil, for 1 h. Then, deionized water was added, little by little, in 200 μL fractions, totaling 800 μL. Then,100 μL of Triton X-100 (Sigma-Aldrich) was added until a paste was obtained.

2.2. Preparation of ZnS, ZnO-S, Ag^0/ZnO-S, Pt^0/ZnO-S and commercial ZnO films

After the paste synthesis step, the ZnS and ZnO-S photoelectrodes were prepared on conductive substrate (FTO-glass) from Aldrich with surface resistivity of 7 Ω/sq and dimensions 1.0 × 3.0 cm^2. Each piece of FTO-glass was previously washed in an ultrasonic bath in three successive steps of 15 min each, followed by a mixture of deionized water and neutral soap, deionized water and isopropyl alcohol, respectively. The preparation of the films consisted of depositing the ZnS paste on the substrate, on the conductive face of the FTO-glass, in an area delimited by 1 cm^2 and 40 μm thick adhesive tape, using the Doctor-Blade method. After drying at room temperature for about 10 min, the samples were heat treated in a muffle furnace with air flow at temperatures of 100, 200, 300, 400, 500, and 600 °C for 2 h. To comparison effect, an uncalcined ZnS film was used as a standard.

To compare the stability and photoelectrocatalytic activity with all ZnO-S films, a commercial zinc oxide film (ZnO, 99.0 % purity, Scientific Exodus) was prepared in a similar way to ZnS, and calcined only at 600 °C. The surface of the ZnO-S films was modified with silver (Ag0) or platinum (Pt0) obtained by photoreduction of a 1.0 × 10^{-3} mol L^{-1} solution of silver nitrate ($AgNO_3$) or hexachloroplatinic acid hexahydrate ($H_2PtCl_6{\cdot}6H_2O$), respectively [41]. In photoreduction, the ZnO-S films were immersed in precursor solutions of Ag^+ or Pt^{4+} in a glass beaker of 10 mL for 10 s. These films were then exposed to UV irradiation in a closed container with three STARLUX® 20 W lamps, placed about 40 cm from the UV source for 5 min. After that, the films were washed various times with deionized water to ensure the complete

removal of excess metal ions.

2.3. Structural and optical characterization of photoelectrodes

X-ray Diffraction (XRD) analysis of ZnS, ZnO-S, Ag^0/ZnO-S, and Pt^0/ZnO-S samples were recorded employing a LabX XRD-6000 diffractometer (Shimadzu, Japan) with Cu-Kα radiation ($\lambda = 0.15406$ nm) at 40 kV and 30 mA, in the range of 2θ from 10° to 110° with a scan speed of 1° min^{-1}. Standard diffractions were compared with data from the American Mineralogist Crystal Structure Database (AMCSD) and Inorganic Crystal Structure Database (ICSD). The Thermogravimetric Analysis (TGA) and Differential Scanning Calorimetry (DSC) experiments were carried out in simultaneous equipment (model 822- Mettler. These thermal studies of sample (initial mass: 18.44 mg) were carried out in an oxidizing atmosphere of synthetic air, with a flow rate of 100 mL min^{-1} and heating rate of 5 °C min^{-1}. The optical properties were registered by a Shimadzu UV-2600 spectrophotometer, using FTO-glass as a reference onto an integrating sphere with barium sulfate between interval wavelength from 800 to 200 nm. The band gap energy of the semiconductor was estimated by the Tauc method from the UV–Vis transmittance curves [42].

2.4. Morphological and photoelectrochemical characterization

The morphology, thickness of the samples, and elemental analysis were characterized by Scanning Electron Microscopy (SEM) coupled to the Energy Dispersive X-ray Spectrometer (EDS) (JEOL EDS System, model 6010LA) with acceleration voltage between 0.5 and 30 kV. The highest resolution images were obtained by *Field Emission Gun Scanning Electron Microscopy* (FEG-SEM, JEOL JSM- 6701F), with a detection limit of around 1 % (m/m) and acceleration voltage of 0.5 to 30 kV. *X-ray Excited Photoelectron Spectroscopy* (XPS, K-alpha+ model, Thermo Fisher Scientific, operating with Al-kα X-ray source) was employed to investigate the elemental composition, chemical and electronic state of the elements present on the surface of the samples. The pressure in the analysis chamber was approximately 10^{-7} Pa, the spot size was 400 μm. The pass energies were 50 eV and 20 eV for the survey and high-resolution spectra, respectively. C1s element was used as reference at 284.8 eV.

The photoelectrochemical properties were studied by using an electrochemical cell formed by optical glass window. The working electrodes were ZnS, ZnO-S, Ag^0/ZnO-S, Pt^0/ZnO-S, and commercial ZnO, (with a geometric area of 1 cm^2); Pt wire was the counter electrode and the Ag/AgCl (aqueous solution of KCl 3.0 mol L^{-1}) was the reference electrode (in a Luggin capillary). A system configured with three electrodes was used, and an aqueous solution of Na_2SO_4 0.1 mol L^{-1} (pH=5.6) was used as an inert support electrolyte. Measurement was performed on a Galvanostat/Potentiostat (Autolab PGSTAT 302-N Metrohm), connected to the NOVA 1.7 software, in the dark and under polychromatic irradiation. Metallic vapor lamp (HQI-TS EXCELLENCE NDL-150 W), with an irradiance adjusted to 100 mW cm^{-2} was used to irradiate the films, to verify the photoelectrocatalytic activity of the films for progesterone degradation.

Cyclic voltammograms with a scan rate of 20 mV s^{-1} was performed (in the dark and under irradiation condition) in order to get the photocurrent values. Flat band potential (E_{fb}) using the Butler-Gärtner model was obtained [43–47], with base on Linear Sweep Voltammetry (LSV) technique in the anode potential range of −0.2 to 1.0 V at a sweep rate of 2.0 mV s^{-1} with chopped illumination every 10 s. For comparison, the potential values recorded (vs. Ag/AgCl) were adjusted in relation to the reversible hydrogen electrode (RHE) according to the Eq. (1) [46,47]:

$$E(\text{vs.RHE}) = \text{E(vs.Ag / AgCl)} + 0.0591\text{V} \times \text{pH} + 0.199\text{V} \quad (1)$$

Furthermore, the potentials after adjusting for the RHE (in volts) were converted to electron-volts (eV) using the Eq. (2) [46]:

$$E(\text{eV}) = \left[-4.5\text{eV} - \text{eE}_{(RHE)} \right] \quad (2)$$

2.5. Progesterone degradation studies

The photocatalytic activity of ZnO-S, commercial ZnO, Ag^0/ZnO-S, and Pt^0/ZnO-S films was analyzed using progesterone solution in initial concentration (C_0) of 0.31 mg L^{-1} in Na_2SO_4 0.1 mol L^{-1} (pH 5.6) as supporting electrolyte, considering three different configurations:

i) Photolysis, which consists of irradiating the solution containing the hormone and using only clean FTO glass immersed in the solution;
ii) Heterogeneous photocatalysis (HP), which uses films of different oxides immersed in the organic pollutant solution;
iii) Electrochemically assisted heterogeneous photocatalysis (EHP). In this configuration, while the system was irradiated, the films (electrodes) remained polarized at 0.70 V (vs Ag/AgCl).

For progesterone degradation studies, was used an electrochemical cell with 15 mL capacity, which was placed at a distance of 12 cm from the irradiation source, adjusted to in 100 mW cm^{-2}. Previous studies, developed by our group, revealed that the spectral profile of polychromatic light is mostly in the visible region [48]. During the photocatalytic this investigation, the system was not stirred and the temperature was maintained at 25 ± 3 °C.

Progesterone photodegradation kinetics was performed after 30 min of adsorption-desorption equilibrium. The system remained irradiated for 3 h and aliquots were collected at successive intervals. Progesterone removal was evaluated based on the intensity of the absorption band that occurs in the UV–Vis spectrum at 248 nm. Thus, the degradation efficiency (η) was determined according to the Eq. (3) [46]:

$$\eta = \frac{A_0 - A_t}{A_0} \quad (3)$$

in this equation, A_0 corresponds to the initial absorbance and A_t represents the absorbance of the progesterone after the irradiation time.

3. Results and discussion

3.1. Structural and optical characterization

Thermogravimetric Analysis (TGA) and Differential Scanning Calorimetry (DSC) were performed for the ZnS suspension (Fig. 1). From TGA analysis, it is possible to see mass losses of 30 and 24% at temperatures between 70 and 100 °C and 170 - 423 °C, which can be attributed to water elimination and PEG decomposition, respectively. A residual mass of 46 % was registered for ZnS initial suspension. The DSC curves show a thermal process involving an endothermic signal that extends up to 100 °C, associated with water elimination. Other thermal signals with exothermic processes were observed with maximums at 221, 530, and 581 °C. The DSC exothermic peak at 221 °C is consistent with PEG decomposition, while the signals at 530 and 581 °C can be attributed to the phase transition from ZnS to ZnO and greater crystallization of the materials, respectively. To confirm this phase transition from ZnS to ZnO, structural characterization was carried out using XRD, and further processing of the data using the Rietveld method.

The structural characterizations by XRD were performed for films and powdered samples. Fig. 2 shows the XRD patterns for ZnS and ZnO-S films. Diffraction signals for pure ZnS film (uncalcined) and those calcined at temperatures from 100 °C to 400 °C are in good agreement with the sphalerite cubic structure of ZnS, with F-43 m space group (ICSD No. 110). However, for the sample calcined at 500 °C, it is possible to observe the appearance of diffraction signals associated to the hexagonal wurtzite phase of ZnO, P63mc space group (ICSD No. 65,119). As

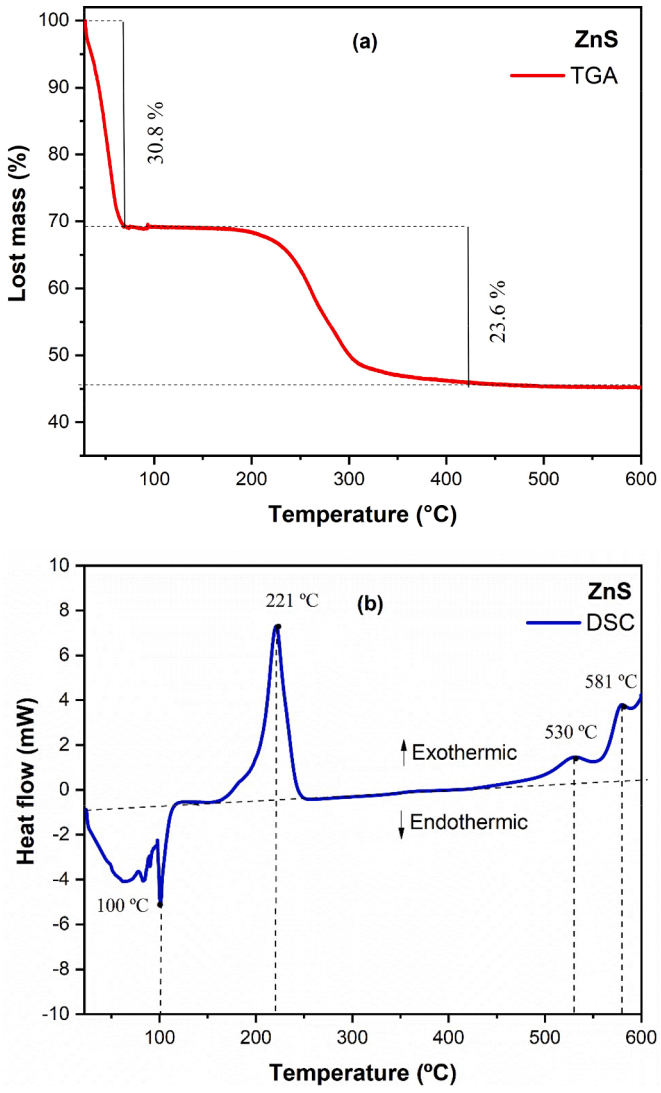

Fig. 1. Thermogravimetric Analysis - TGA and Differential Scanning Calorimetry - DSC for pure ZnS sample with synthetic airflow.

displayed in Fig. 2**b**, these signals were intensified for samples annealed at 600 °C, with planes (100), (002), and (101) attributed to ZnO with wurtzite hexagonal phase, indicating that ZnS was converted to ZnO-S. The signals at 2θ equal to 26.43°, 33.80°, 37.88°, 51.45°, 61.55°, and 65.61° are attributed to the FTO-glass, being observed in all film samples. The structural characterization revealed that during the heat treatment process occurred change of cubic ZnS phase for the wurtzite hexagonal ZnO phase at 600 °C. In addition, XRD signals of hexagonal ZnO were clearly evidenced at 500 °C. Considering the XRD data and temperatures treatment of 100 - 600 °C observed in TGA/DSC is possible entry of oxygen into host lattice ZnS with thermal treatment, from here, these samples will be denoted as ZnS-O1, ZnS-O2, ZnS-O3, ZnS-O4, ZnO-S5, and ZnO-S6, respectively.

Diffractograms without the interference of the FTO-glass diffraction signals were obtained for powder samples. The Rietveld refinement results for samples calcined from 100 to 600 °C are shown in **Fig. S2.** Schematic representations of the ZnS and ZnO-S6 unit cells are shown in **Fig. S3**, as well as the Rietveld refinement parameters are presented in **Table S1**. In the sample calcined at 600 °C, practically all the sulfur was replaced by oxygen atoms, leaving only a few sulfur atoms in the crystalline structure of ZnO, resulting in zinc oxide doped with sulfur (ZnO-S), verified by the XRD and Rietveld refinement for sample powders (**Figures S1 and S2**).

Previous studies have shown that the surface modification of oxide films with metallic particles improves the charge separation process in electrodes [46]. Considering that the film treated at 600 °C was the one that presented the most complete phase transition from ZnS to ZnO, the ZnO-S6 film was chosen for modification with metallic nanoparticles. Also, for comparison purposes, a commercial ZnO film was prepared and investigated. Fig. 2**c** shows diffractogram for ZnO-S6, Ag^0/ZnO-S6, Pt^0/ZnO-S6 and ZnO (commercial) films calcined at 600 °C. The apparent diffraction patterns for all samples are in agreement with wurtzite phase. In addition, characteristic diffraction planes of the cubic structure of Ag^0 and Pt^0 metallic NPs produced by photoreduction were observed on the ZnO-S films, according to ICSD N°. 22,434 and ICSD No. 243,678, respectively [41,46].

The average crystallite size (D) for the pure ZnS and ZnO-S samples was estimated from the Debye-Scherrer equation, as shown in Eq. (4) [46]:

$$D = \frac{K\lambda}{\beta.Cos\theta} \quad (4)$$

where K is Scherrer's constant, which represents the form factor (K = 0.91) [49], λ is the wavelength of the radiation used (Cu-Kα), β is the width at half height of the peak, and θ is the diffraction angle. For the ZnS sample, the average crystallite size was calculated employing the (111), (022), and (113) diffraction signals, located at 2θ = 28.59 °, 47.58 °, and 56.33 ° respectively. On the other hand, for the ZnO-S6 film, D was calculated from the (100), (002), and (101) peaks at 31.78 °, 34.44 °, and 36.29 ° respectively. The average crystallite size showed results very similar, which were estimated at 31 and 30 nm for ZnS and ZnO-S films, respectively.

Fig. 3 shows the optical behavior for all films, investigated by UV–Vis spectroscopy. Studies show that the ZnO microcrystal presents light absorption at wavelengths close to 380 nm, which corresponds to E_{BG} of 3.2 eV [15,50]. In contrast, ZnS is a semiconductor with an exceptionally large E_{BG}, between 3.5 and 3.7 eV, and has absorption of light in the UV–Vis region, at a wavelength of less than 350 nm [17].

Fig. 3**a** shows the UV–Vis curves, recorded in the transmittance mode for ZnS film in comparison to that on calcined at different temperatures. As observed in Fig. 3**a,** the thermal treatment caused a displacement of the absorption edge towards the higher wavelengths. This result indicates that the ZnO-S6 sample has a greater capacity to absorb radiation at longer wavelengths, suggesting that the remaining sulfur in the oxide structure acts as a doping and promotes the formation of energy levels between the valence and conduction bands of the semiconductor. Furthermore, as indicated by the DSC curves and structural characterization by XRD, increasing the heat treatment temperature promotes the formation of ZnO phase.

From the transmittance curves obtained by spectroscopy in the UV–Vis region, it was possible to estimate the band gap energy (E_{BG}) for all samples using the Tauc method [51], according to Eq. (5):

$$\alpha h\nu = A(h\nu - -E_{BG})^{1/2} \quad (5)$$

where A is the proportionality constant, h is Planck's constant, ν the frequency of light, E_{BG} is the band gap energy, α is the absorption coefficient near the absorption edge and ½ is applied due to the direct transition of the material. Both ZnS and ZnO have a direct gap and these curves usually have a linear part, which can be extrapolated to estimate the semiconductor E_{BG} [45,46]. Thus, the curves obtained from $(\alpha h\nu)^2$ as a function of $h\nu$ are shown in Figs. 3**b** and 3**c**. The estimated E_{BG} values for pure ZnS (3.52 eV) and commercial ZnO (3.25 eV) films are close to those already mentioned in previous studies, with energy ranging from 3.5 to 3.7 eV for ZnS and 3.2–3.4 eV for ZnO [15,17].

As observed from DSC and XRD analysis (Figs. 1 and 2), from 500 °C it is possible to identify phase transition and conversion of ZnS into ZnO. However, this transition was completed with sample annealing at 600 °C. The ZnO-S6 film, therefore, presented E_{BG} (3.14 eV) lower than pure

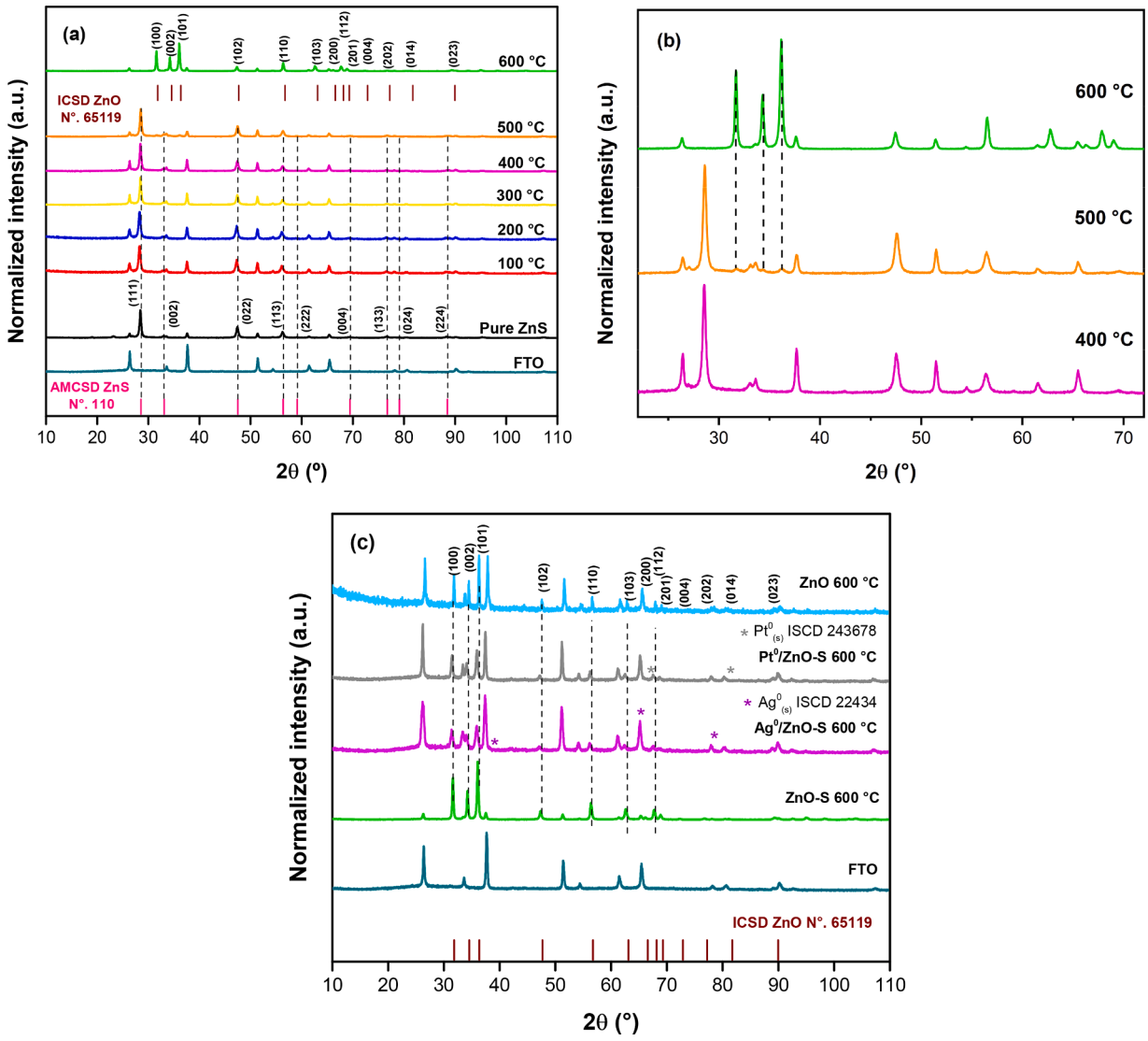

Fig. 2. XRD standard of: (a) pure ZnS films (non-calcined) and heat treated at temperatures of 100 °C, 200 °C, 300 °C, 400 °C, 500 °C and 600 °C per 2 h, (b) appearance of planes (010), (002) and (011) in the phase change from cubic ZnS to hexagonal ZnO and (c) films of ZnO-S 600 °C, Ag^0/ZnO-S 600 °C, Pt^0/ZnO-S 600 °C and ZnO (commercial) 600 °C. Vertical bars indicate the positions of the cubic ZnS (AMCSD No. 110) and ZnO (ICSD No. 65,119) planes.

ZnO in its wurtzite crystalline phase, indicating a possible incorporation of sulfur in the crystalline structure of ZnO. This occurred because the thermal conversion of ZnS to ZnO happened with substitutions of oxygen atoms in a position initially occupied by sulfur atoms. However, this change would not be complete, as some sulfur atoms remain in the ZnO structure, acting as impurities in the ZnO crystal. Thus, the materials obtained can be considered S-doped ZnO (ZnO-S), with sulfur occupying substitutional positions in the semiconductor structure.

In principle, doping caused a decrease in E_{BG} due to an enlargement of the VB and to the presence of states located between the VB and CB, resulting in an improvement in electron injection from the VB to CB of the material [45–48]. Fig. 3**c** shows the Tauc plot only for films prepared at 600 ºC. The small variation in E_{BG} values indicates that the presence of Ag^0 and Pt^0 nanoparticles does not alter the structure of ZnO-S or ZnO oxides, as occurs in doping processes [41,46]. Previous studies have shown that E_{BG} calculated for oxide films generally presents higher values than those calculated for the material in powder form. To assess this issue, UV–Vis spectra in diffuse reflectance mode were obtained for the powders of ZnS (pure) and ZnO-S (calcined). The E_{BG} values were estimated by the Kubelka-Munk function, which is calculated by plotting the square product of the absorption coefficient and energy $(\alpha E)^2$ versus energy E, $((\alpha E)^2$ vs E) (**See Fig. S4**). Table 1 summarizes the calculated E_{BG} values for the different samples.

3.2. *Chemical composition and morphological characterization*

The films were prepared by spreading the ZnS paste on a FTO-glass, by the Doctor Blade method, delimited by an area of 1.0 cm^2. Pure ZnS and the calcined films showed a particle density of about 2.6 ± 0.4 mg cm^{-2}. The SEM images showed that for samples calcined at a temperature lower than 600 ºC, the films presented similar morphology, formed by agglomerates of almost spherical particles with ca. 6 μm. However, the ZnO-S6 film shows a distinct morphology, with particles formed by smaller structures like plates. Various SEM images can be observed in Supporting Information. The SEM images in Fig. S5 show that the cross section of the films calcined from 100 to 500 °C have a thickness of about 14±2 μm. On the other hand, the ZnO-S6 electrode has a smaller thickness, with an average value of 7.1 ± 0.8 μm. This lower ZnO-S6 thickness value may be associated with the oxidation of the ZnS precursor, corroborating the TGA curves presented in Fig. 1**a**. Fig. 4 displays the morphological characterization and EDS mapping/spectra of the films calcined at 600 ºC, in comparison to ZnS film. Based on the EDS

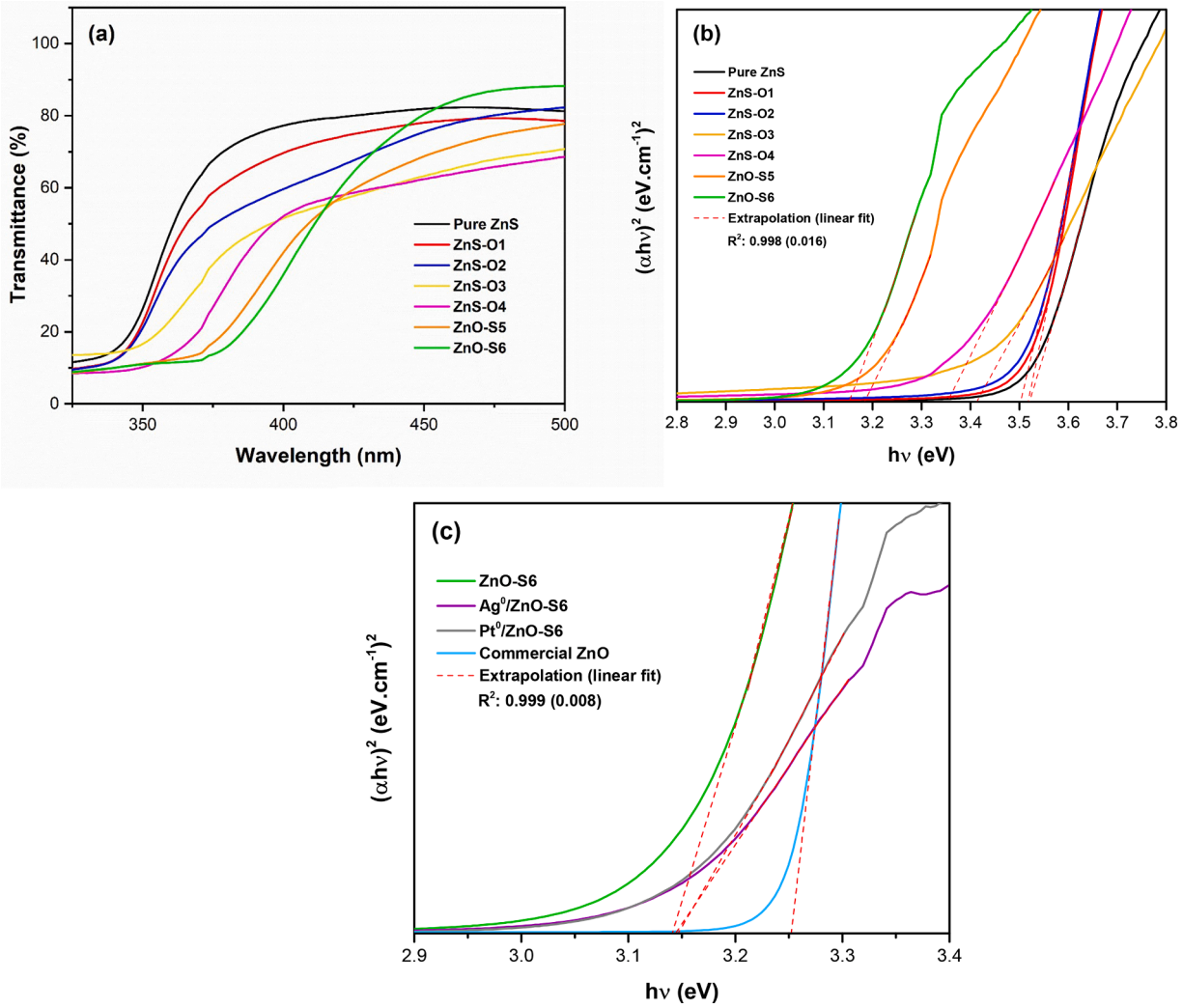

Fig. 3. UV–Vis curves for pure and calcined films at temperatures from 100 to 600 °C: (a) transmittance; (b) E_{BG} values estimated by the Tauc method for ZnS (pure and calcined); (c) EBG values estimated by the Tauc method for ZnO-S, Ag^0/ZnO-S, Pt^0/ZnO-S and commercial ZnO films.

Table 1
Optical band gap values for pure ZnS, ZnO-S6, Ag^0/ZnO-S6, Pt^0/ZnO-S6 and commercial ZnO films, calculated from the transmittance curves obtained by spectroscopy in the UV–Vis region by the Tauc method.

Samples	E_{BG} / eV
ZnS puro	3.52
ZnS-O1	3.52
ZnS-O2	3.50
ZnS-O3	3.41
ZnS-O4	3.35
ZnO-S5	3.18
ZnO-S6	3.14
Ag^0/ZnO-S6	3.14
Pt^0/ZnO-S6	3.14
Commercial ZnO	3.25

spectra and mapping analysis it was possible to identify the presence and homogeneous distribution of Zn, O, S, Ag, and Pt atoms on the surface of samples (ZnS, ZnO-S6, commercial ZnO and Ag^0/ZnO-S6, Pt^0/ZnO-S6 films).

The EDS analysis for ZnS film identified the presence of Zn and S. Also, a small signal associated to O atoms was registered for ZnS surface sample. The presence of oxygen can be attributed to the precursors used in the preparation of semiconductor suspensions, such as PEG 20,000 and Triton X-100. With the heat treatment at 600 °C, there was a reduction in the intensity of the S signal and a consequent increase in the O signal. Also, the mapping carried out in the ZnO-S6, Ag^0/ZnO-S6, and Pt^0/ZnO-S6 samples revealed a homogeneous distribution of Zn, O, S, Ag, and Pt on the surface of the samples. However, it was not possible to observe evidence of metallic nanoparticles on the surface of the functionalized films, probably due to the small size of these particles. For comparison purposes, the SEM-EDS analysis was also performed for commercial ZnO film prepared at 600 °C. The EDS analysis identified the Zn and O atoms on the semiconductor surface, uniformly distributed. Sulfur was not detected.

Fig. 5 presents images of the surface morphology of the ZnS and ZnO-S6 films, taken at higher magnification. The images show similar morphology already discussed in **Fig. S5**. In the pure ZnS film (Fig. 5**a-b**), irregular shaped structures can be seen immersed in a "pasty" material, which can be associated with PEG 20,000 and Triton X-100 unburned, present in the precursor suspension. In the highest magnification image, it was observed that the surface morphology of the ZnS film is formed by very irregular structures, forming an agglomerate of particles of different shapes, such as nanoplates and irregular nanospheres [52]. The ZnO-S6 film (Fig. 5**c-d**) showed particles with hedgehog-like morphology that are formed as a result of the growth of nanoplates that densely cover the surface of microspheres [53]. The size

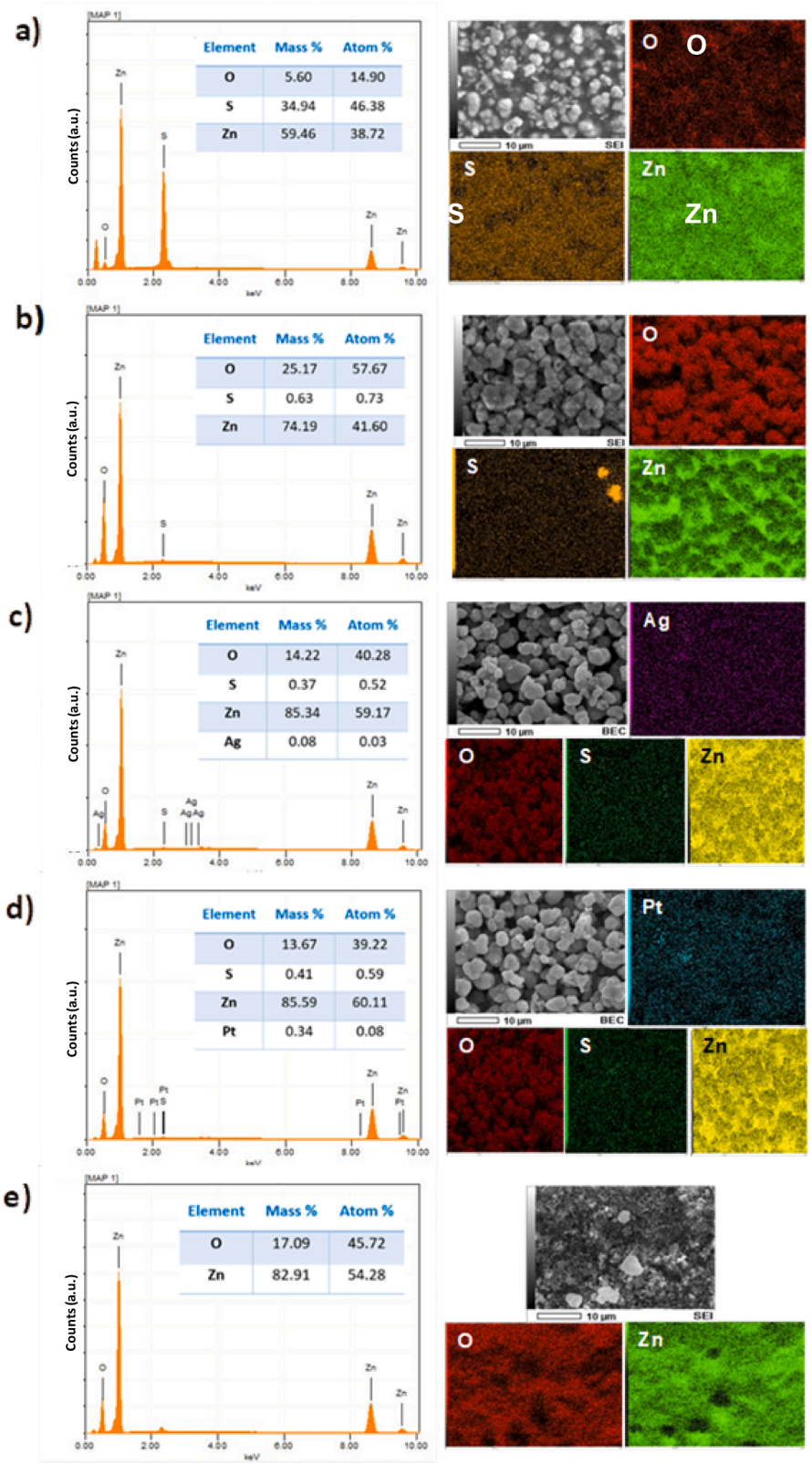

Fig. 4. SEM surface images of pure ZnS (a), ZnO-S6 (b), Ag^0/ZnO-S6 (c), Pt^0/ZnO-S6 (d), and commercial ZnO (e) films; with mapping and distribution of Zn, O, S, Ag and Pt atoms on the electrode surface, obtained by EDS.

of nano-hedgehogs ranges from 100 to 400 nm.

Fig. 6 shows XPS survey spectrum and high-resolution XPS spectra over Zn 2p, S 2p, O 1 s, Ag 3d, and Pt 4f peaks of films. The survey scan spectrum (Fig. 6**a)** shows the presence of peaks corresponding to Zn, S, O, and C for ZnS, ZnO-S6, Pt^0/ZnO-S, and commercial ZnO films. High-resolution XPS spectra corresponding to Zn 2p, S 2p, O 1 s, Ag 3d, and Pt 4f are shown from Figs. 6**b-f.** Fig. 6**b**, the high-resolution Zn 2p spectra display two well-defined peaks with average binding energy of 1021.06

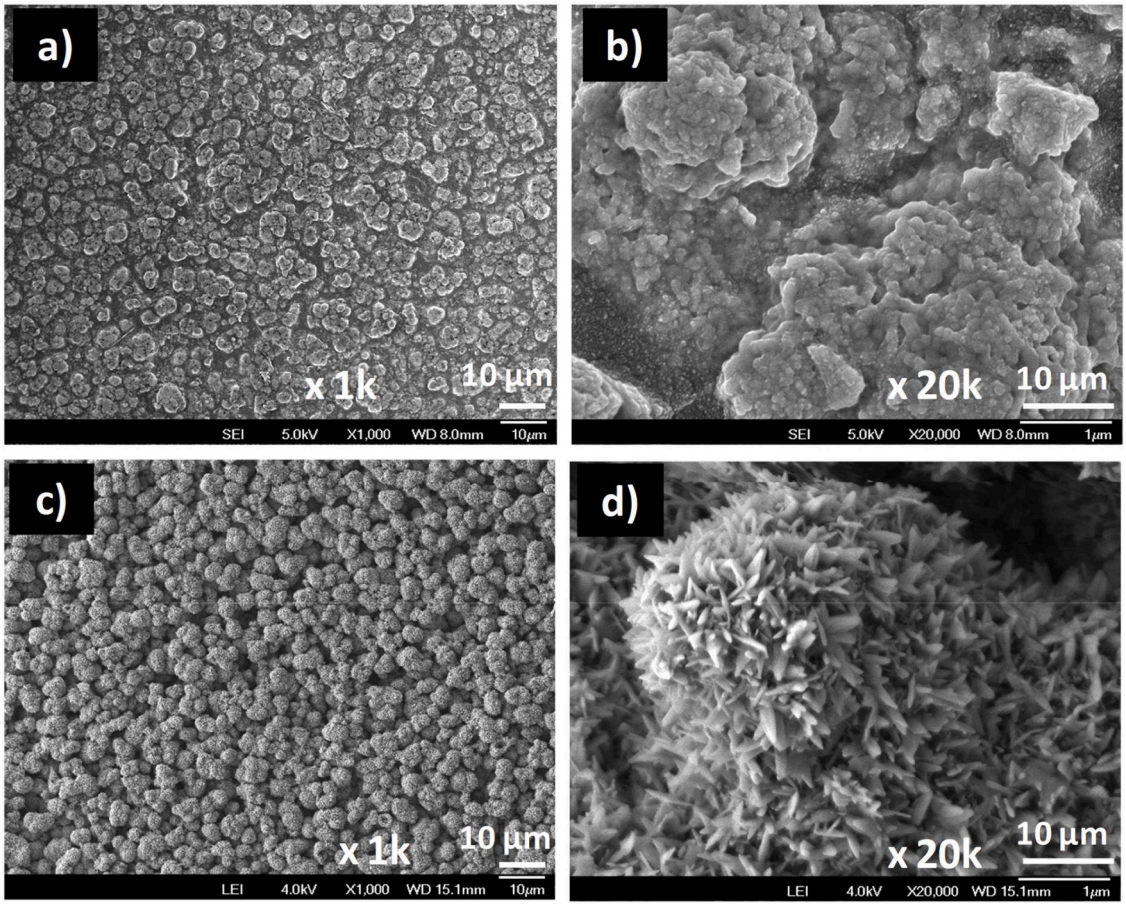

Fig. 5. Surface images of pure ZnS (a-b) and ZnO-S6 films (c-d) obtained by FEG-SEM, with magnification of 1k, and 20k, respectively.

eV and 1044.18 eV attributed to the presence of Zn^{2+} and corresponding to Zn $2p_{3/2}$ and Zn $2p_{1/2}$, respectively [54]. This separation peaks with ΔE of 23 eV is in agreement with previously reported values for zinc ions binding to sulfur ions in ZnS networks [55].

The asymmetrical S 2p peak in Fig. 6**c** has been deconvoluted into two subpeaks corresponding to S $2p_{3/2}$ and S $2p_{1/2}$, which are located at 160.31 and 161.30 eV, respectively [56]. The doublet for the no calcined sample can be attributed to S^{2-} ions in a crystalline lattice of the ZnS structure. The sample calcined at 100 °C (ZnS-O1) presents a small shift in the maxima in the S $2p_{3/2}$ and S $2p_{1/2}$ signals towards lower energy values, which can be attributed to species with S-S and O-S bonds present on the ZnS surface [57]. However, for samples calcined at 200 to 600 °C, the appearance of a second doublet was observed, which can be attributed to defects caused by the thermal treatment of ZnS. Previous study shows that thermal treatment can cause sulfur vacancies in ZnS, which result in defects in the crystalline structure of zinc sulfide [58]. It is important to note that the second doublet maintains a 2:1 ratio, as expected for the signal ratio (S $2p_{3/2}$: S $2p_{1/2}$), obeying the degeneracy rule [59]. Based on Fig. 6**d**, it can be seen that for samples calcined at 600 °C, there is a drastic reduction in the signal attributed to S^{2-} ions, suggesting that at this temperature almost all the sulfur in the initial structure of ZnS was exchanged for oxygen atoms, leading to the formation of ZnO with some S atoms as impurities.

Fig. 6**e** shows the deconvolution from peak to O 1 s, indicating peaks with binding energy values in 528.82 and 530.57 eV. These peaks correspond to the lattice oxygen of ZnO, OH^- or adsorbed oxygen species O^- and O^{2-}, respectively [60]. This result confirms the formation of anions on the surface, which is the most important surface reaction, related to the detection phenomenon.

Further deconvolution of Ag 3d peaks in Fig. 6**g** revealed the presence of signals of Ag $3d_{5/2}$ and Ag $3d_{3/2}$, centered at 365.91 and 371.89 eV, respectively. The division of the spin-orbit peaks of the 3d doublet of Ag was 5.98 eV, together with typical binding energy values (the standard binding energy of Ag $3d_{5/2}$ is about 368.2 eV), suggests the formation of metallic silver on the of the ZnO-S6 film surface, in addition to the asymmetry between the peaks, which confirms metallic silver rather than of eventual silver oxide (Fig. 6**g**) [32].

Fig. 6**h** shows XPS spectrum for Pt 4f signal. An adequate deconvolution of the signal was performed considering an energy variation of 3.3 eV (peak-to-peak distance) and full width at half maximum (FWHM), according to procedures presented in previous studies [61,62]. Based on deconvolution, two doublets were found for the platinum signal. The first doublet with peaks of Pt $4f_{7/2}$ and Pt $4f_{5/2}$ centered at 70.79 and 74.09 eV were attributed to the metallic state of platinum (Pt^0). The second doublet was attributed to platinum in the 4+ oxidation state (Pt^{4+}), which may be associated with non-photoreduced H_2PtCl_6 precursors during the surface modification of the ZnO-S6 film.

3.3. Photoelectrochemical analysis

Fig. 7 shows the cyclic voltammetry curves obtained for pure ZnS film in comparison to that one treated thermally from 100 to 600 °C. The measurement was performed under conditions of dark or polychromatic irradiation with a sweep speed of 20 mV s^{-1} in a potential window ranging from −0.2 to 1.0 V, limited by O_2 and H_2 gas release reactions.

From the under light/dark conditions, it was possible to determine the type of semiconductor for all films. In the dark, all films showed an open circuit potential (V_{OC}) of approximately 0.02 V, when irradiated the V_{OC} value decreased to −0.25 V. The observed change of V_{OC} to negative values is characteristic of *n*-type semiconductors. In *n*-type

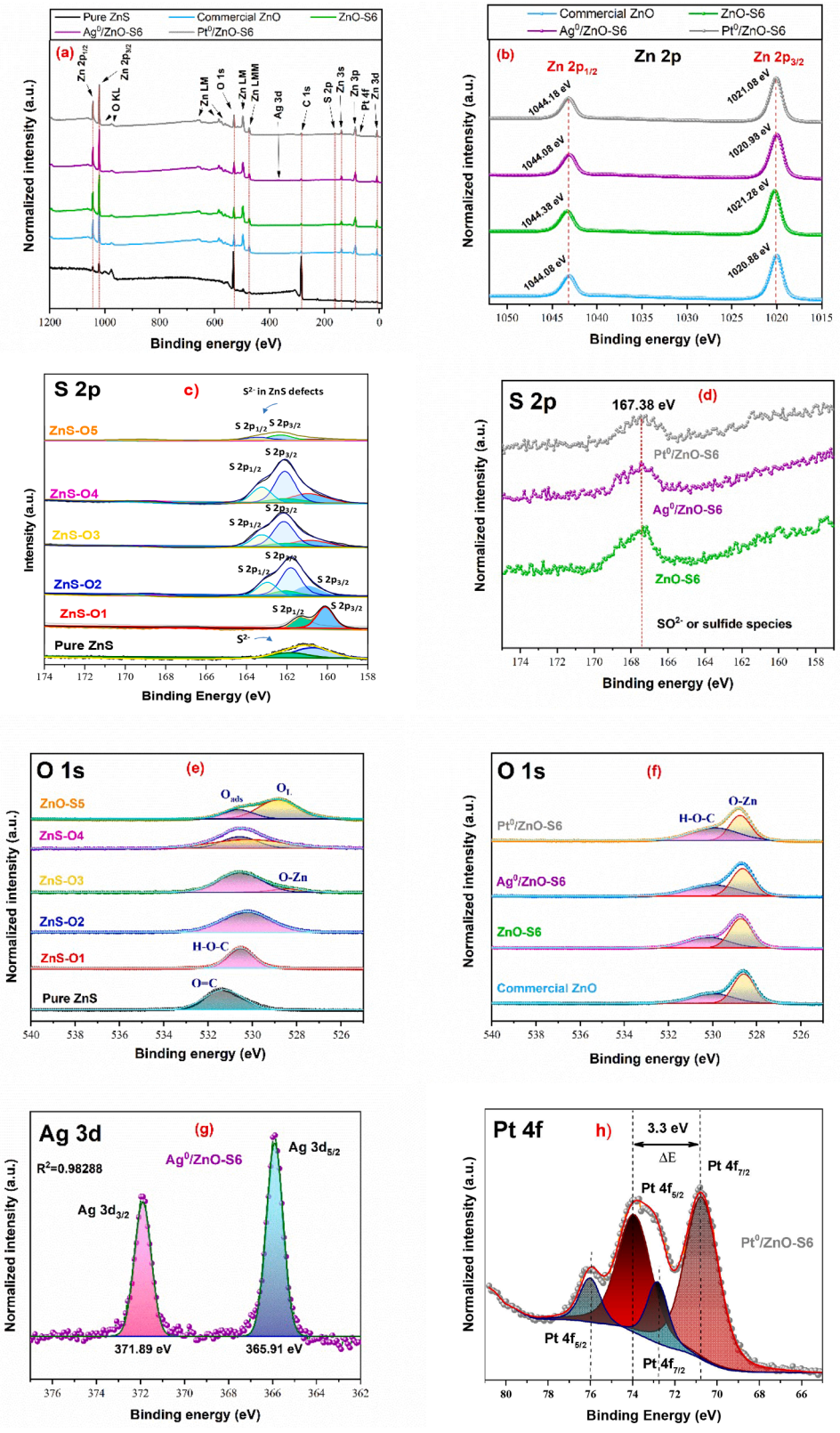

Fig. 6. XPS spectrum: a) Survey of pure ZnS in comparison to ZnO-S6, commercial ZnO, Ag^0/ZnO-S6, and Pt^0/ZnO-S6 films; b) level core spectrum for Zn 2p; c) high resolution XPS spectra of S 2p for films of pure ZnS film in comparison to calcined from 100 to 500 °C; d) S 2p for films of 600 °C; e) O 1 s for films of pure ZnS in comparison to calcined from 100 to 500 °C; f) O 1 s for films calcined at 600 °C; g) XPS spectra of Ag 3d for Ag^0/ZnO-S6 and h) Pt 4f for Pt^0/ZnO-S6 film.

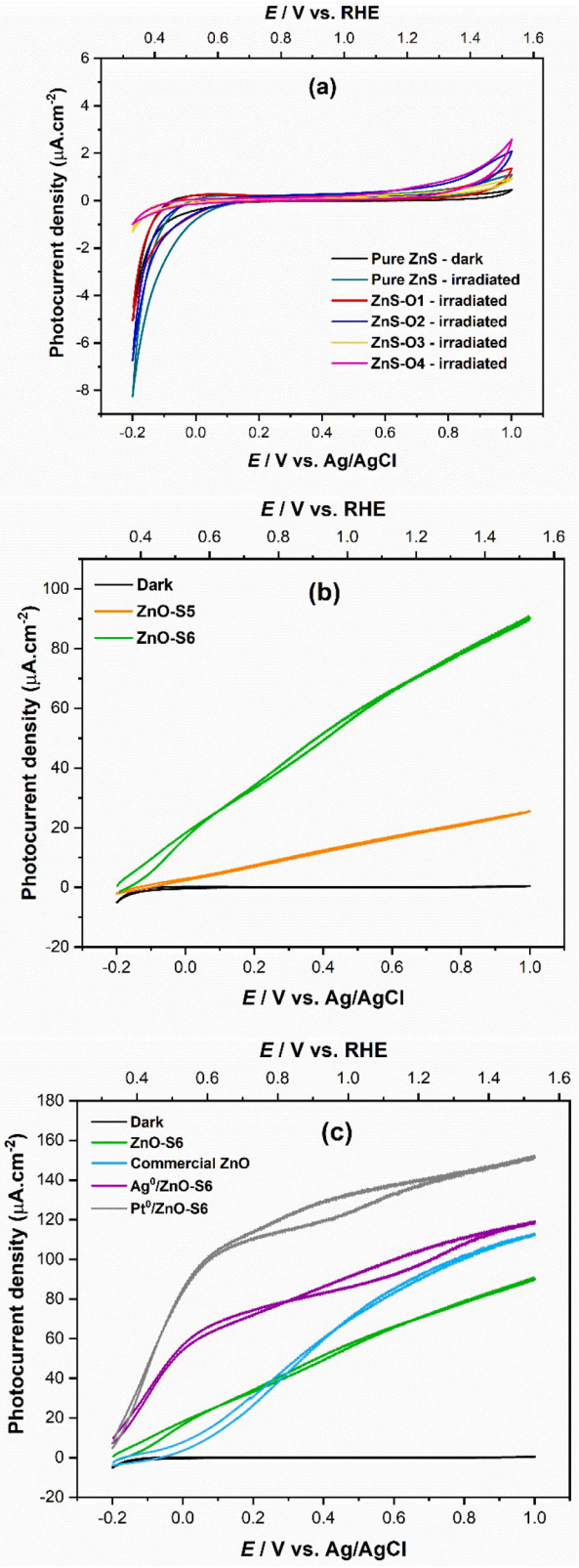

Fig. 7. Cyclic voltammetry ($V = 20$ mV s^{-1}) in 0.1 mol L^{-1} Na_2SO_4 aqueous solution in the dark and under polychromatic irradiation for (a) pure ZnS films and samples treated during 120 min at 100 °C, 200 °C, 300 °C and 400 °C; (b) films treated during 120 min at 500 °C and 600 °C (ZnO-S); and (c) films of ZnO-S6 in comparison to commercial ZnO, Ag^0/ZnO-S6 and Pt^0/ZnO-S6 treated at 600 °C for 120 min.

semiconductors, holes move to the electrode surface and oxidize the species in solution, producing an anodic photocurrent when the semiconductor is irradiated [45–48]. In the dark, a current of approximately zero was observed for all films, considering the potential window adopted.

According to Fig. 7**a,** the pure ZnS film and calcined from 100 to 400 °C, displayed low photocurrent values. However, the ZnO-S5 and ZnO-S6 films (Fig. 7**b),** show photocurrent values of about 10 and 65 μA cm^{-2}, respectively (at 0.70 V vs Ag/AgCl). The highest photocurrent value for the ZnO-S6 film indicates greater crystallinity for this material, corroborating the XRD analyses. Considering the EDS and XPS analysis, at 600 °C, almost all the sulfur atoms were substituted by oxygen atoms. Thus, some sulfur atoms present an impurity (doping) in substitutional positions to the oxygen atoms, resulting in S doping ZnO sample. The introduction of S^{2-} ions changes the energy of the semiconductor band gap, its ability to absorb radiation with longer wavelengths, and improved the charge separation process.

Subsequently, all photoelectrochemical studies were conducted with films calcined at 600 °C (ZnO-S6), considering this film displayed a photocurrent density four times greater than the film calcined at 500 °C. The ZnO-S6 electrodes were functionalized with nanoparticles of silver (AgNP) or platinum by the photoreduction method. The presence of metallic NPs on the surface of the ZnO-S6 film increased the photocurrent value, reaching 105 μA cm^{-2} for Ag^0/ZnO-S6 and 140 μA cm^{-2} for the Pt^0/ZnO-S6 films, respectively. An increase in photocurrent density was obtained for both functionalized films investigated, probably due to the interaction of Zn O-S particles with Ag^0 and Pt^0 NPs. In previous work, Valenti et al. [63] reported the improvement of photoelectrochemical behavior using a $CuWO_4$ electrode modified by Au nanoparticles as the electrode. This improvement was correlated to a combination of factors such as Plasmonic Resonance Energy Transfer (PRET), light scattering and electron injection. Thus, the gain in current value is due to metallic NPs, since these act as light-scattering centers or electron traps. If the reaction kinetics of the hole with species contained in the solution is faster compared to the recombination process of the e^-/h^+ pair, the photogenerated electrons are moved through the grain boundaries of the constituent crystallites of the film, reach the conductive substrate are collected by the external circuit [45,46]. Fig. 7**c** also shows the curve for the commercial ZnO film, with a photocurrent of 1.3 times higher than the ZnO-S6 film at 0.7 V (vs. Ag/AgCl). This commercial ZnO film was used as a comparative parameter in relation to the ZnO-S6 film for several analyses performed in this work.

Fig. 8 shows linear voltammograms from −0.3 to 1.0 V vs Ag/AgCl for ZnO-S6, Ag^0/ZnO-S6, and Pt^0/ZnO-S6, films, with light interruption (chopper at 0.10 Hz) and registered at 2 mV s^{-1} of scan rate. From these curves, the flat band potential (E_{fb}) was obtained for ZnO-S6, commercial ZnO, Ag^0/ZnO-S6 and Pt^0/ZnO-S6 films (inset in Fig. 8**a-d).** E_{fb} is considered an approximation of Fermi level potential and expresses for *n*-type semiconductors the reducing power of the electrons in CB, making it possible to estimate its application in photoelectrocatalytic processes [64,65]. E_{fb} values were determined by Butler-Gartner model according to previous studies by our research group [45–48]. The E_{fb} values for the ZnO-S6, commercial ZnO, Ag^0/ZnO-S6 and Pt^0/ZnO-S6 electrodes are −0.09 V, −0.21 V and −0.17 V and 0.07 V vs Ag/AgCl respectively.

Fig. 9**a** shows cyclic voltammograms, obtained in the dark, for progesterone in different concentrations. In this voltammograms, this possible observe an oxidation peak with an onset potential of 0.87 V and a maximum peak of 1.05 V for the solution with 0.50 mmol L^{-1} of progesterone.

In order to prove that this response is related to progesterone, cyclic voltammograms were performed for more dilute solutions in the supporting electrolyte. Thus, the response related to each diluted solution was registered until the extinction of the signal. The observed oxidation potential related to progesterone was transformed on the energy scale applying Eqs. (1) and (2), in which the value of −6.0 eV was obtained. In

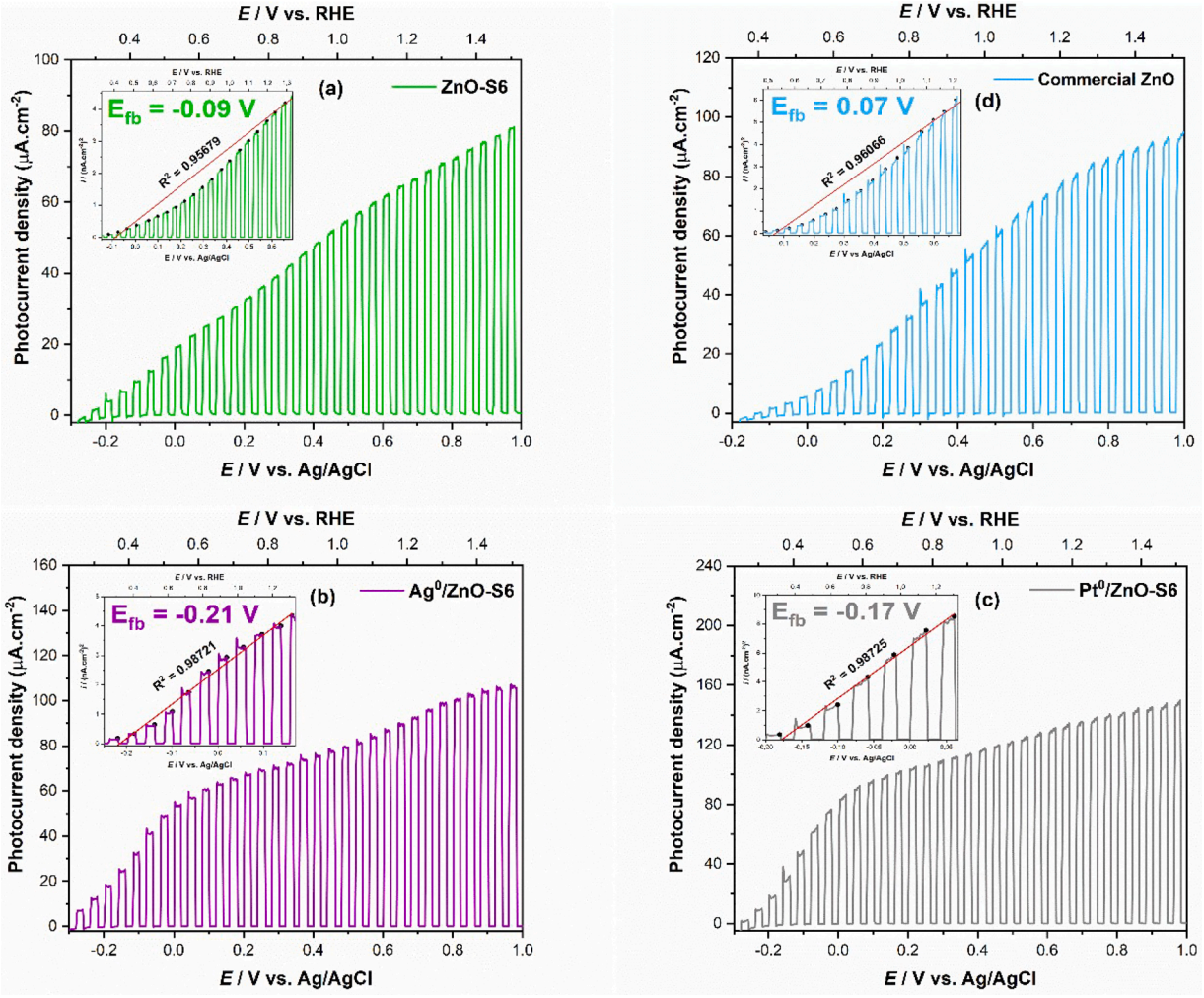

Fig. 8. Linear voltammetry curves of the electrodes (a) ZnO-S6, (b) Ag^0/ZnO-S6, (c) Pt^0/ZnO-S6 and (d) commercial ZnO, illuminated with chopped polychromatic light (10 s) in an 0.1 mol L^{-1} Na_2SO_4 aqueous solution. Inset: i^2 vs. V curves by Butler-Gartner Model.

the case of organic compounds, the maximum oxidation value can be associated to the highest occupied molecular orbital (HOMO). Also, inset in Fig. 9**a,** there is an absorption UV–Vis curve for progesterone, which represents the energy gap between HOMO and LUMO (lowest unoccupied molecular orbital) of this pollutant. An absorption band at 248 nm, was observed and related to the progesterone UV–Vis absorption spectrum. According to [E(eV)=1241/ λ(nm)], the relative energy value is 5.0 eV. Considering this referred value to the gap energy in progesterone, the LUMO level corresponds to −1.08 eV. From the E_{BG}, E_{fb}, progesterone oxidation potential, and UV–Vis values, the relative positions of the semiconductor conduction/valence band edges, and oxidation potential positions were estimated using the methodology shown previously. Fig. 9**b** displays the progesterone oxidation potential compared to the VB and CB edge potentials of each film. The diagram shows the relative position of the VB and CB edges, which are favorable for progesterone oxidation. Whereas the VB edge displays more positive potential, highest in relation to the HOMO level of the pollutant, the photogenerated holes in the VB cause the oxidation of progesterone. According to Fig. 9**b**, all films calcined at 600 ºC have similar potentials for oxidation of progesterone as a pollutant. However, ZnO-S6 films modified with Ag and Pt should be more efficient because they have higher photocurrent values.

3.4. Progesterone degradation

The photocatalytic response of the ZnO-S6, commercial ZnO, Ag^0/ZnO-S6 and Pt^0/ZnO-S6 was investigated for the degradation of the hormone progesterone in aqueous medium, using systems with heterogeneous photocatalysis (HP) and electrochemically assisted heterogeneous photocatalysis (EHP) configurations. For the EHP condition, the films were biased at 0.70 V (vs Ag/AgCl). Fig. 10 displays the degradation efficiency of hormone under polychromatic irradiation, as well as the degradation kinetics related to the photocatalytic process.

As observed in Fig. 10**a,** the first step corresponds to the adsorption process on the surface of the photocatalyst for about 30 min, due to the fact that system is not illuminated. However, with polychromatic irradiation, the hormone concentration reduced with time due to the formation of photogenerated oxidant species in the system [66]. The degradation efficiency of progesterone by photolysis was only 3.82 % under irradiation for 3 h. However, in HP and EHP arrangements, the efficiency reached higher values, especially in the EHP form. In the HP configuration, ZnO-S6, Ag^0/ZnO-S6, Pt^0/ZnO-S6 and commercial ZnO, electrodes increased the degradation efficiency of 10.05 %, 10.63 %, 11.52 %, and 9.35 %, respectively, for the same irradiation time. On the other hand, for the EHP configuration, the photoelectrodes showed a higher degradation efficiency of 40.40 %, 45.11 %, 50.80 %, and 30.36 %, respectively (Table 2).

Compared to commercial ZnO film, unmodified ZnO-S6 films and those modified with metal NPs improved the degradation of progesterone in both conditions (EHP and HP). The photoexcited electrons to the BC (after irradiation) were trapped by the metallic NPs, thus, inhibiting the recombination of the e^-/h^+ pair [67]. In addition, the surface

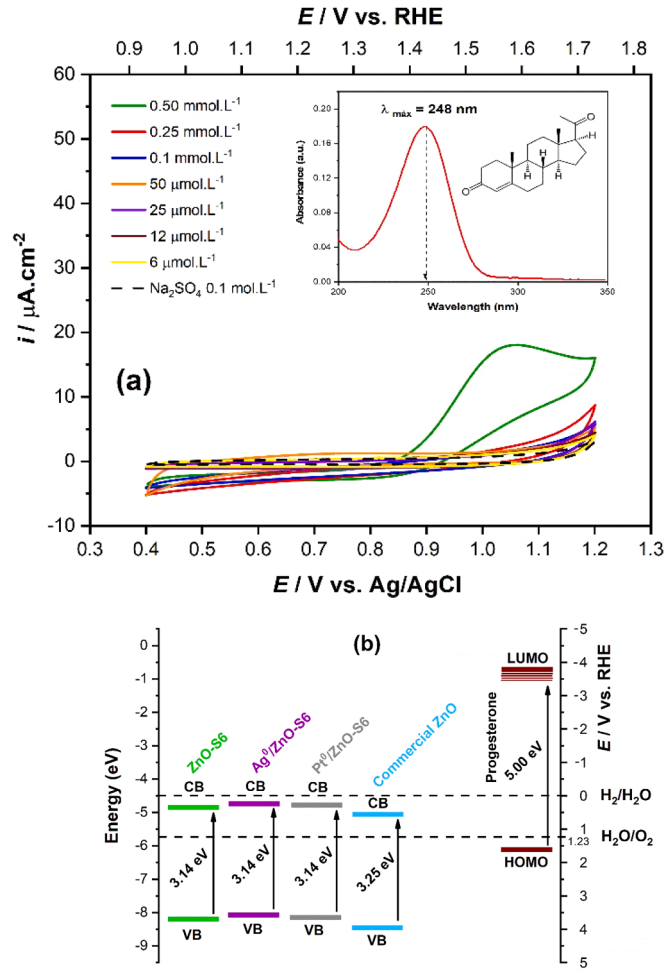

Fig. 9. (a) Cyclic voltammograms (10 mV s^{-1}) for platinum electrode in the dark, in aqueous solution of Na_2SO_4 0.1 mol.L^{-1} as supporting electrolyte containing different concentrations of progesterone; (b) Energy diagram for the semiconductor/progesterone hormone interface in aqueous solution, considering the highest occupied and the lowest unoccupied molecular orbitals, as well as the edges of the valence and conduction bands for the electrodes.

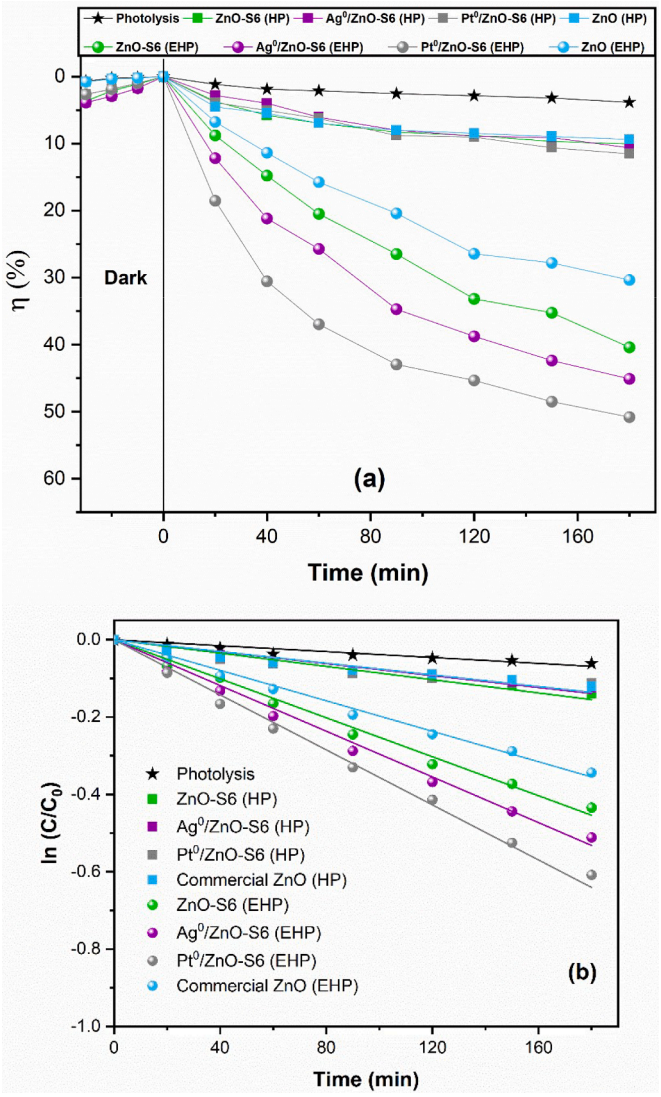

Fig. 10. Efficiency in the degradation of progesterone in aqueous solution during polychromatic irradiation (25 ± 2 °C) by photolysis, Heterogeneous Photocatalysis (HP) and electro-assisted HP (EHP) for ZnO-S6, Ag^0/ZnO-S6, Pt^0/ZnO-S6 and ZnO commercial electrodes, (b) kinetic of degradations.

plasmonic resonance and the light scattering fomented by NPs (Ag^0 and Pt^0) in ZnO-S films improved photocatalytic activity [68]. In the EHP arrangement, under potential application, the electrodes are polarized. Thus, when the *n*-type semiconductor is irradiated, electrons are conducted towards the conductive substrate, improving the charge separation process. In addition, Oliveira *et al.* [69] presented better responses for TiO_2 and TiO_2/WO_3 electrodes investigated in EHP configuration to the photocatalytic remediation of 17-α-ethinylestradiol in solution, as the technique performs a faster and lower cost degradation.

Some strategies have been reported in the literature to degrade progesterone from water, for instance: photolysis by UVA light, oxidation with potassium permanganate, photoeletrocatalysis electrochemically assisted degradation, among other techniques [70–72]. However, as mentioned earlier, photodegradation employing S-doped ZnO films in the EHP configuration has not been reported in the literature.

In general, the degradation reactions of organic compounds follow the model of Langmuir-Hinshelwood (L-H) defined by Eq. (6) [46]:

$$r = \frac{dc}{dt} = \frac{kK_c}{1 + K_c} \tag{6}$$

where *r* is the initial rate of photooxidation, *C* is the reagent concentration, *t* is its time of irradiation, *k* is the rate constant and K_C is the adsorption constant of the species in solution. This L-H model can be simplified considering systems with single species and at low concentrations. As seen in Fig. 9**b**, the progesterone degradation in solution can be fitted to pseudo-first order kinetics, which obeys the simplest model described by Eq. (7) [46]:

Table 2
Catalytic efficiency and degradation kinetic of the progesterone in different systems.

Photocatalyst Film	Catalytic System	Catalytic Efficiency η (%)	Degradation Kinetc k (min^{-1})
	Photolysis	3.82	3.32×10^{-4}
ZnO-S6	HP	10.05	5.82×10^{-4}
	EHP	40.40	2.14×10^{-3}
Ag^0/ZnO-S6	HP	10.63	6.42×10^{-4}
	EHP	45.11	2.29×10^{-3}
Pt^0/ZnO-S6	HP	11.52	6.74×10^{-4}
	EHP	50.80	2.44×10^{-3}
Commercial ZnO	HP	9.35	5.64×10^{-4}
	EHP	30.36	1.69×10^{-3}

$$r = \frac{A_t}{A_0} = -kt \quad (7)$$

where k corresponds to a degradation rate constant of the hormone (min^{-1}), and t represents the irradiation time (min). Thus, the values related to the progesterone photodegradation were fitted to a graph of ln (A_t/A_0) vs. time in order to get the rate constant **(**Fig. 10**b).** The *k* values for the removal of progesterone, as well as the degradation efficiency, are specified in Table 2. According to the results, the *k* values are in accordance with the degradation efficiency, that is, the greater the value of *k*, the higher degradation efficiency. The highest *k* values were obtained in the EHP configuration. After functionalization with Ag^0 and Pt^0 NPs, slightly higher values of *k* were obtained for Ag^0/ZnO-S6 and Pt^0/ZnO-S6 films, respectively.

Generally speaking, the success of the photodegradation of hormones is associated to several factors, for example: the capacity of photodegradation of estrogenic steroidal hormones, physicochemical properties, initial concentrations of the pollutants, photon flux, light source, catalyst loading, type, temperature, pH, among others [71].

The progesterone presents relatively low solubility in water (8.81 mg L^{-1} at 25 °C) [46], therefore the analyses could not be carried out with progesterone solutions of higher concentrations. In fact, hormones can be considered persistent pollutants and these results showed that the progesterone in aqueous medium is not easily degraded by photolysis alone.

Compared with commercial ZnO electrode, sulfur-doped ZnO films exhibited higher progesterone degradation capacity in HP and EHP configurations.. Comparing all electrodes in the HP and EHP configurations, those functionalized with metallic NPs exhibited greater progesterone degradation efficiency, however, the Pt^0 electrode /ZnO-S electrode presented the highest capacity for progesterone degradation, which may be related to a greater distribution of platinum NPs deposited compared to silver on the surface of ZnO-S, as can be seen in Fig. 4. According to the literature, Pt^0 NPs act as one of the more efficient load transfer facilitators [41,46].

Surface plasmon resonance corresponds to an efficient procedure to localize photon absorption on the surface of the semiconductor, by the incorporation of NPs of the plasmonic metal in the semiconductor material. The frequency and intensity of plasmonic resonance depend on the geometry, distribution engineering of NPs, and dielectric property of the surrounding environment [46].

The superior performance related to progesterone degradation (51 %) was verified for the Pt^0/ZnO-S electrode in the EHP configuration. In comparison to the commercial ZnO film, the S-doped ZnO film showed superior catalytic performance for progesterone removal. The characterizations indicate that the doping of ZnO with S introduces new energy levels in the E_{BG}, which favors the transfer of electrons to CB, resulting in holes in the VB that react with the pollutant on the surface of the semiconductor, causing its oxidation.

In summary, these results are promising, considering that progesterone is a neutral molecule and difficult to degrade. Therefore, it is possible to conclude that the EHP form is more proper compared to HP and photolysis under polychromatic light to degrade the progesterone solution in an aqueous medium. Fig. 11 shows the separation process of photogenerated e^-/h^+ pairs. This indicates that more charge carriers generated participate in the photoelectrochemical activity due to the presence of metal NPs at the semiconductor interface, for the generation of reactive •OH and other species for the degradation of progesterone. Thus, the presented results indicate that the S-doped ZnO film presents good morphological and interesting structural and optical properties, and these are advanced when the structure is modified by functionalization using metallic NPs. However, the improvement in the photoelectrochemical performance of the ZnO-S6 electrode for the photocatalytic degradation of organic pollutants in aqueous solution (such as progesterone) is associated to the transfer efficiency of photogenerated charges, improved light absorption, and reduction in the

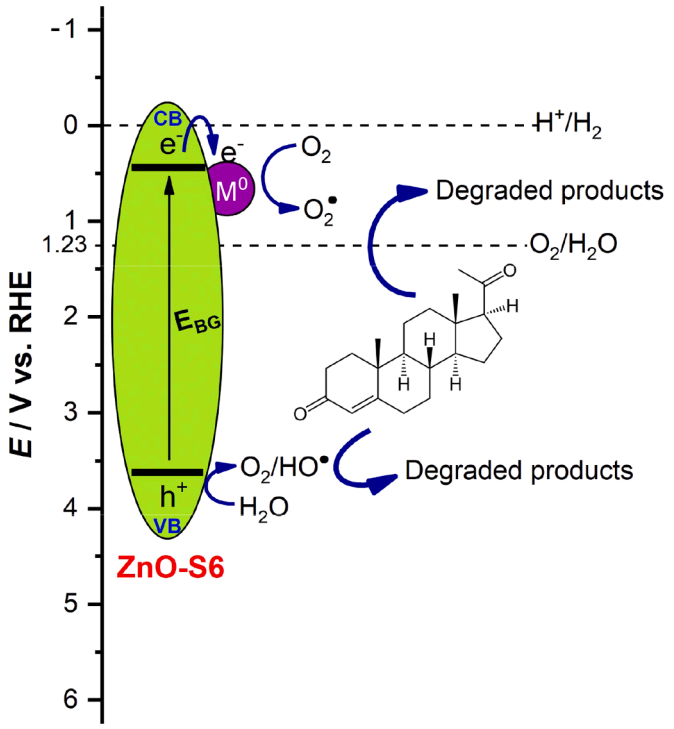

Fig. 11. Schematic illustration of the mechanism of charge separation and photocatalytic process over photocatalyst under irradiation of visible light.

recombination rate of the photogenerated e^-/h^+ pair. Furthermore, structural evaluation of the ZnO-S6 material obtained by XRD measurement carried out after the electrocatalytic progesterone degradation process revealed that the wurtzite phase of the oxide remains, revealing that the photocatalyst material has good stability (see **Fig. S6**)

4. Conclusion

This work revealed that ZnO-S films can be prepared by the Doctor-Blade method at temperature of 600 °C in the course of 2 h, and functionalized with Ag^0 and Pt^0 (NPs) by photoreduction. Pure and calcined ZnS films at 100 to 400 °C exhibited a cubic structure. At 500 °C, two phases were observed (cubic and hexagonal) for ZnS sphalerite and ZnO wurtzite, respectively and the film calcined at 600 °C showed only a hexagonal phase of ZnO. Pure ZnS samples and those calcined up to 500 °C exhibited irregular spherical morphology, however, the sample calcined at 600 °C showed a coating of nanosheets over the irregular spheres. A decrease in the direct optical E_{BG} (calculated by the Tauc method) was evidenced during the thermal treatment and shift of light absorption toward the visible region. The XPS data showed signals of Zn2p, S2p, O1s, Ag3d, and Pt4f on ZnS and ZnO-S films. Photoelectrochemical investigations indicate that doping and functionalization with metallic NPs accelerate the electron transport, increasing the charge separation, thus reducing recombination of the photogenerated e^-/h^+ pair. In this way, oxidative degradation of progesterone in aqueous medium with polychromatic irradiation was studied in HP and EHP configurations using ZnO-S6, commercial ZnO, Ag^0/ZnO-S6, and Pt^0/ZnO-S6 electrodes as photocatalyst for 3 h. When the photoanode was biased at + 0.7 V, the photocatalytic efficiency increased, probably because the application of potential suppressed the charge recombination. So, the highest photocatalytic response was observed for the EHP arrangement for the Pt^0/ZnO-S6 electrode, due to doping with S and the presence of nanoparticles on the surface of the electrode. Therefore, functionalized ZnO-S6 films with metallic NPs can be considered promising materials as a photoanode and the EHP configuration can provide information for further studies on PEC applications in water

separation and photodegradation of organic pollutants.

Data availability

No data was used for the research described in the article.

CRediT authorship contribution statement

Jailson S. Luis: Conceptualization, Methodology, Investigation, Data curation, Writing – original draft, Writing – review & editing, Visualization. **Samuel S. Eduardo:** Conceptualization, Methodology, Validation, Formal analysis, Investigation. **Maria J.S. Costa:** Formal analysis, Investigation, Data curation, Writing – original draft, Formal analysis, Writing – review & editing. **Luciano C. Brandão-Lima:** Resources, Methodology, Investigation. **Renato A. Antunes:** Formal analysis, Methodology, Investigation. **Raphael O. Ferreira:** Conceptualization, Methodology, Investigation. **Rejane M.P. Silva:** Resources, Methodology, Investigation, Visualization. **Reginaldo S. Santos:** Conceptualization, Methodology, Writing – review & editing, Supervision, Project administration.

Declaration of competing interest

The authors declare that they have no known competing financial interests or personal relationships that could have appeared to influence the work reported in this paper.

Acknowledgments

The authors would like to thank the research funding agencies CAPES and CNPq for the scholarships granted to the post-graduate students participating in the study and other financial support. Also, thanks to CCN2-PPGCM-UFPI-LIMAV, FAPESP-CDMF for their technical support.

Supplementary materials

Supplementary material associated with this article can be found, in the online version, at doi:10.1016/j.molstruc.2024.137764.

References

[1] D. Gielen, F. Boshell, D. Saygin, M.D. Bazilian, N. Wagner, R. Gorini, The role of renewable energy in the global energy transformation, Energy Strategy Rev. 24 (2019) 38–50, https://doi.org/10.1016/j.esr.2019.01.006.
[2] H. Song, S. Luo, H. Huang, B. Deng, J. Ye, Solar-Driven hydrogen production: recent advances, challenges, and future perspectives, ACS. Energy Lett. 7 (2022) 1043–1065, https://doi.org/10.1021/acsenergylett.1c02591.
[3] V. Sharma, M. Prasad, P. Ilaiyaraja, C. Sudakar, S. Jadkar, Electrodeposition of highly porous ZnO nanostructures with hydrothermal amination for efficient photoelectrochemical activity, Int. J. Hydrogen. Energy 44 (2019) 11459–11471, https://doi.org/10.1016/j.ijhydene. 2019.03.132.
[4] D. Nanakaraju, B.D. Glass, M. Oelgemoller, Advanced oxidation process-mediated removal of pharmaceuticals from water: a review, J. Environ. Manage. 219 (2018) 189–207, https://doi.org/10.1016/j.jenvman.2018.04.103.
[5] J. Wang, Z. Wang, C.L.Z. Vieira, J.M. Wolfson, G. Pingtian, S. Huang, Review on the treatment of organic pollutants in water by ultrasonic technology, Ultrason. Sonochem. 55 (2019) 273–278, https://doi.org/10.1016/j.ultsonch.2019.01.017.
[6] M. Patel, R. Kumar, K. Kishor, T. Mlsna, C.U. Pittman Jr., D. Mohan, Pharmaceuticals of emerging concern in aquatic systems: chemistry, occurrence, effects, and removal methods, Chem. Rev. 119 (2019) 3510–3673, https://doi.org/10.1021/acs.cherev8b00299.
[7] J.O. Ojoghoro, A.J. Chaudhary, P. Campo, J.P. Sumpter, M.D. Scrimshaw, Progesterone potentially degrades to potent androgens in surface waters, Sci. Total Environ. 579 (2017) 1876–1884, https://doi.org/10.1016/j.scitotenv.2016.11.176.
[8] L. Kolatorova, J. Vitku, J. Suchopar, M. Hill, A. Parizek, Progesterone: a steroid with wide range of effects in physiology as well as human medicine, Int. J. Mol. Sci. 23 (2022) 7989, https://doi.org/10.3390/ijms23147989.
[9] R. Kant, C. Dwivedi, S. Pathak, V. Dutta, Fabrication of ZnO nanostructures using al doped ZnO (AZO) templates for application in photoelectrochemical water splitting, Appl. Surf. Sci. 447 (2018) 200–212, https://doi.org/10.1016/j.apsusc.2018.03.208.
[10] W. Ye, F. Chen, F. Zhao, F. Han, Y. Li, $CuWO_4$ nanoflake arrays based single-junction and heterojunction photoanodes for photoelectrochemical water oxidation, ACS Appl. Mater. Interfaces 8 (2016) 9211–9217, https://doi.org/10.1021/acsami.6b03176.
[11] Z. Weng, H. Guo, X. Liu, S. Wu, K.W.K. Yeung, P.K. Chu, Nanostructured TiO_2 for energy conversion and storage, RSC. Adv. 3 (2013) 24758–24775, https://doi.org/10.1039/C3RA44031A.
[12] A. Manohar, J. Park, D.D. Geleta, C. Krishnamoorthi, R. Thangam, H. Kang, J. Lee, Synthesis and characterization of ZnO nanoparticles for photocatalysis, antibacterial and cytotoxicity in kidney cancer (A498) cell lines, J. Alloys. Compd. 874 (2021) 159868, https://doi.org/10.1016/j.jallcom.2021.159868.
[13] A. Baranowska-Korczyc, M. Kościński, E.L. Coy, B.F. Grześkowiak, M. Jasiurkowska-Delaporte, B. Peplińska, S. Jurga, ZnS coating for enhanced environmental stability and improved properties of ZnO thin films, RSC. Adv. 8 (2018) 24411–24421, https://doi.org/10.1039/C8RA02823K.
[14] R.S. Carneiro, M.R. Canuto, L.K. Ribeiro, D.C.L. Ferreira, A.F.C. Assunção, C.A.C. B. Costa, J.D. Freitas, M. Rai, L.S. Cavalcante, W.S. Alves, A.L.M.M. Filho, J. F. Silva, R.S. Santos, V.T. Uchôa, Novel antibacterial efficacy of ZnO nanocrystals/Ag nanoparticles loaded with extract of Ximenia americana L. stem bark for wound healing, South Afric. J. Botany 151 (part A) (2022) 18–32, https://doi.org/10.1016/j.sajb.2022.09.030.
[15] R. Qin, F. Meng, M.W. Khan, B. Yu, H. Li, Z. Fan, J. Gong, Fabrication and enhanced photocatalytic property of TiO_2-ZnO composite photocatalysts, Mater. Lett. 240 (2019) 84–87, https://doi.org/10.1016/j.matlet.2018.12.139.
[16] N. Salah, A. Hameed, M. Aslam, M.S. Abdel-Wahab, S.S. Babkair, F.S. Bahabri, Flow controlled fabrication of N doped ZnO thin films and estimation of their performance for sunlight photocatalytic decontamination of water, Chem. Eng. J. 291 (2016) 115–127, https://doi.org/10.1016/j.cej.2016.01.111.
[17] S. Biswas, S. Kar, Fabrication of ZnS nanoparticles and nanorods with cubic and hexagonal crystal structures: a simple solvothermal approach, Nanotechnology. 19 (2008) 045710, https://doi.org/10.1088/0957-4484/19/04/045710.
[18] S. Lee, S. Jeong, D. Kim, S. Hwang, M. Jeon, J. Moon, ZnO nanoparticles with controlled shapes and sizes prepared using a simple polyol synthesis, Superlattices. Microstruct. 43 (2008) 330–339, https://doi.org/10.1016/j.spmi.2008.01.004.
[19] E. Broitman, C. Bojorge, F. Elhordoy, V.R. Kent, G.Z. Gadioli, R.E. Marotti, H. R. Canepa, E.A. Dalchiele, Comparative study on the properties of ZnO nanowires and nanocrystalline thin films, Surf. Coat. Technol. 213 (2012) 59–64, https://doi.org/10.1016/j.surfcoat.2012.10.015.
[20] N.R. More, U.B. Chanshetti, B. Aurangabad, S. Dnyaneshwar, M. Newasa, Review article on ZnO thin films by spray pyrolysis, Int. J. Chem. Phys. Sci. 7 (2018) 51–54.
[21] Q. Li, J. Bian, J. Sun, J. Wang, Y. Luo, K. Sun, D. Yu, Controllable growth of well-aligned ZnO nanorod arrays by low-temperature wet chemical bath deposition method, Appl. Surf. Sci. 256 (2010) 1698–1702, https://doi.org/10.1016/j.apsusc.2009.09.097.
[22] C. Rodwihok, S. Choopun, P. Ruankham, A. Gardchareon, S. Phadungdhitidhada, D. Wongratanaphisan, Uv sensing properties of ZnO nanowires/nanorods, Appl. Surf. Sci. 477 (2019) 159–165, https://doi.org/10.1016/j.apsusc.2017.11.056.
[23] M. Laurenti, V. Cauda, Porous zinc oxide thin films: synthesis approaches and applications, Coatings 8 (2018) 67, https://doi.org/10.3390/coatings8020067.
[24] A.M. Qadir, I.Y. Erdogan, Structural properties and enhanced photoelectrochemical performance of ZnO films decorated with Cu_2O nanocubes, Int. J. Hydrogen. Energy 44 (2019) 18694–18702, https://doi.org/10.1016/j.ijhydene.2019.01.101.
[25] G. Redmond, D. Fitzmaurice, M. Graetzel, Visible Light Sensitization by cis-Bis (thiocyanato)bis(2,2'-bipyridyl-4,4'-dicarboxylato)ruthenium(II) of a Transparent Nanocrystalline ZnO Film Prepared by Sol-Gel Techniques, Chem. Mater. 6 (1994) 686–691, https://doi.org/10.1021/cm00041a020.
[26] A.I. Kontos, A.G. Kontos, D.S. Tsoukleris, M.C. Bernard, N. Spyrel- lis, P. Falaras, Nanostructured TiO_2 films for dsscs prepared by combining doctor-blade and sol–gel techniques, J. Mater. Process. Technol. 196 (2008) 243–248, https://doi.org/10.1016/j.jmatprotec.2007.05.051.
[27] X. Liu, Y. Luo, H. Li, Y. Fan, Z. Yu, Y. Lin, L. Chen, Q. Meng, Room temperature fabrication of porous ZnO photoelectrodes for flexible dye-sensitized solar cells, Chem. Commun. 284 (2007) 2847–2849, https://doi.org/10.1039/B700472A.
[28] L. Song, J. Hu, X. Lu, Z. Lu, J. Xie, A. Hao, Y. Cao, Boosting the Photocatalytic Activity and Resistance of Photostability of ZnS Nanoparticles, Inorg. Chem. 61 (2022) 8217–8225, https://doi.org/10.1021/acs.inorgchem.2c00632.
[29] M. Pirhashemi, A. Habibi-Yangjeh, S.R. Pouranb, Review on the criteria anticipated for the fabrication of highly efficient ZnO-based visible-light-driven photocatalysts, J. Indus. Eng. Chem. 62 (2018) 1–25, https://doi.org/10.1016/j.jiec.2018.01.012.
[30] A.S. Gonçalves, S.A.M. Lima, M.R. Davolos, S.G. Antônio, C.O.P. Santos, The effects of $ZnGa_2O_4$ formation on structural and optical properties of ZnO: ga powders, J. Solid. State Chem. 179 (2006) 1330–1334, https://doi.org/10.1016/j.jssc.2006.01.046.
[31] R.S. Santos, G.A. Faria, C. Giles, C.A.P. Leite, H.D.S. Barbosa, M.A.Z. Arruda, C. Longo, Iron insertion and hematite segregation on Fe-Doped TiO_2 nanoparticles obtained from sol-gel and hydrothermal methods, ACS Appl. Mater. Interfaces 4 (2012) 5555–5561, https://doi.org/10.1021/am301444k.
[32] S.M. Hosseini, I.A. Sarsari, P. Kameli, H. Salamati, Effect of Ag doping on structural, optical, and photocatalytic properties of ZnO nanoparticles, J. Alloys Compd. 640 (2015) 408–415, https://doi.org/10.1016/j.jallcom.2015.03.136.
[33] B. Dindar, A.C. Güler, Comparison of facile synthesized N doped, B doped and undoped ZnO for the photocatalytic removal of Rhodamine B, Environmental

Nanotechnology, Monit. Manag. 10 (2018) 457–466, https://doi.org/10.1016/j.enmm.2018.09.001.
[34] A.U.R. Bacha, H. Cheng, J. Han, I. Nabi, K. Li, T. Wang, Y. Yang, S. Ajmal, S. Liu, L. Zhang, Significantly accelerated PEC degradation of organic pollutant with addition of sulfite and mechanism study, Appl. Catal. B Environ. 248 (2019) 441–449, https://doi.org/10.1016/j.apcatb.2019.02.049.
[35] X.Y. Xie, P. Zhan, L.Y. Li, D.J. Zhou, D.Y. Guo, J.X. Meng, Y. Bai, W.J. Zheng, Synthesis of S-doped ZnO by the interaction of sulfur with zinc salt in PEG200, J. Alloys. Compd. 644 (2015) 383–389, https://doi.org/10.1016/j.jallcom.2015.04.214.
[36] T. Mao, M. Liu, L. Lin, Y. Cheng, C. Fang, A study on doping and compound of zinc oxide photocatalysts, Polym. (Basel) 14 (2022) 4484, https://doi.org/10.3390/polym14214484.
[37] K.W. Aga, M.T. Efa, T.T. Beyene, Effects of sulfur doping and temperature on the energy bandgap of ZnO nanoparticles and their antibacterial activities, ACS. Omega 7 (12) (2022) 10796–10803, https://doi.org/10.1021/acsomega.2c00647.
[38] Z.B. Yu, L. Yin, Y. Xie, G. Liu, X. Ma, H.M. Cheng, Crystallinity-dependent substitutional nitrogen doping in ZnO and its improved visible light photocatalytic activity, J. Colloid. Interface Sci. 400 (2013), https://doi.org/10.1016/j.jcis.2013.02.046.
[39] Z. Liu, J. Wu, J. Zhang, Quantum dots and plasmonic Ag decorated WO_3 nanorod photoanodes with enhanced photoelectrochemical performances, Int. J. Hydrogen. Energy 41 (2016) 20529–20535, https://doi.org/10.1016/j.ijhydene.2016.09.055.
[40] G.Z. Bosshard, J.M.S. Silva, S.A.M. Lima, I.O. Mazalia, F.A. Sígoli, Optical properties of polydisperse submicrometer aggregates of sulfur-containing zinc oxide consisting of spherical nanocrystallites, New J. Chem. 35 (2011) 902–908, https://doi.org/10.1039/c0nj00914h.
[41] M.J.S. Costa, G.S. Costa, A.E.B. Lima, E.L. G Jr., E. Longo, L.S. Cavalcante, R. S. Santos, Investigation of charge recombination lifetime in gamma-WO_3 films modified with Ag^0 and Pt^0 nanoparticles and its influence on photocurrent density, Ionics. (Kiel) 24 (2018) 3291–3297, https://doi.org/10.1007/s11581-018-2640-1.
[42] M. Radecka, M. Rekas, A. Trenczek-Zajac, K. Zakrzewska, Importance of the band gap energy and flat band potential for application of modified TiO_2 photoanodes in water photolysis, J. Power. Sources. 181 (2008) 46–55, https://doi.org/10.1016/j.jpowsour.2007.10.082.
[43] W.W. Gärtner, Depletion-layer photoeffects in semiconductors, Phys. Rev. 116 (1959) 84–87, https://doi.org/10.1103/PhysRev.116.84.
[44] M.A. Butler, Photoelectrolysis and physical properties of the semiconducting electrode WO_3, J. Appl. Phys. 48 (1977) 1914–1920, https://doi.org/10.1063/1.323948.
[45] A.E.B. Lima, M.J.S. Costa, R.S. Santos, N.C. Batista, L.S. Cavalcante, E. Longo, E. L. G Jr., Facile preparation of $CuWO_4$ porous films and their photoelectrochemical properties, Electrochim. Acta 256 (2017) 139–145, https://doi.org/10.1016/j.electacta.2017.10.010.
[46] M.J.S. Costa, G.S. Costa, A.E.B. Lima, G.E. Luz Jr, E. Longo, L.S. Cavalcante, R. S. Santos, Photocurrent response and progesterone degradation by employing wo_3 films modified with platinum and silver nanoparticles, Chempluschem. 83 (2018) 1153–1161, https://doi.org/10.1002/cplu.201800534.
[47] G.S. Costa, M.J.S. Costa, H.G. Oliveira, L.C.B. Lima, E.L. G Jr., L.S. Cavalcante, R. S. Santos, Effect of the applied potential condition on the photocatalytic properties of Fe_2O_3/WO_3 heterojunction films, J. Inorg. Organomet. Polym. Mater. 30 (2020) 2851–2862, https://doi.org/10.1007/s10904-019-01429-0.
[48] M.J.S. Costa, A.E.B. Lima, E.P. Ribeiro, G.S. Costa, E. Longo, E.L. G Jr., L. S. Cavalcante, R.S. Santos, Transition metal tungstates AWO_4(A^{2+} = Fe, Co, Ni, and Cu) thin films and their photoelectrochemical behavior as photoanode for photocatalytic applications, J. Appl. Electrochem. 53 (2023) 1349–1367, https://doi.org/10.1007/s10800-023-01851-w.
[49] M. Louhichi, S. Romdhane, A. Fkiri, L.S. Smiri, H. Bouchriha, Structural and photoluminescence properties of Al-doped zinc oxide nanoparticles synthesized in polyol, Appl. Surf. Sci. 356 (2015) 998–1004, https://doi.org/10.1016/j.apsusc.2015.08.202.
[50] C.Y. Tsay, K.S. Fan, Y.W. Wang, C.J. Chang, Y.K. Tseng, C.K. Lin, Transparent semiconductor zinc oxide thin films deposited on glass substrates by sol–gel process, Ceram. Int. 36 (2010) 1791–1795, https://doi.org/10.1016/j.ceramint.2010.03.005.
[51] D.L. Wood, J. Tauc, Weak absorption tails in amorphous semiconductors, Phys. Rev. B 5 (1972) 3144–3151, https://doi.org/10.1103/PhysRevB.5.3144.
[52] X. Fang, T. Zhai, U.K. Gautam, L. Li, L. Wu, Y. Bando, D. Golberg, ZnS nanostructures: from synthesis to applications, Prog. Mater. Sci. 56 (2011) 175–287, https://doi.org/10.1016/j.pmatsci.2010.10.001.
[53] Y.X. Wang, Z.C. Shen, D.D. Huang, Z.S. Yang, High-performance ZnO nanosheets/nanocrystalline aggregates composite photoanode film in dye-sensitized solar cells, Mater. Lett. 214 (2018) 88–90, https://doi.org/10.1016/j.matlet.2017.11.057.
[54] X. Du, H. Zhao, Y. Lu, Z. Zhang, A. Kulka, K. Swierczek, Synthesis of core-shell-like ZnS/C nanocomposite as improved anode material for lithium ion batteries, Electrochim. Acta 228 (2017) 100–106, https://doi.org/10.1016/j.electacta.2017.01.038.
[55] Y.I. Choi, S. Lee, S.K. Kim, Y.I. Kim, D.W. Cho, M.M. Khan, Y. Sohn, Fabrication of ZnO, ZnS, Ag-ZnS, and Au-ZnS microspheres for photocatalytic activities, CO oxidation and 2-hydroxyterephthalic acid synthesis, J. Alloys. Compd. 675 (2016) 46–56, https://doi.org/10.1016/j.jallcom.2016.03.070.
[56] F. Li, M.R. Kaiser, J. Ma, Z.P. Guo, H.K. Liu, J.Z. Wang, Free-standing sulfur-polypyrrole cathode in conjunction with polypyrrole-coated separator for flexible Li-S batteries, Energy Storage Mater. 13 (2018) 312–322, https://doi.org/10.1016/j.ensm.2018.02.007.
[57] D.J. Zhou, X.Y. Xie, Y. l. Zhang, D.Y. Guo, Y.J. Zhou, J.F. Xie, Facile synthesis of ZnS nanorods in PEG and their spectral performance, Mater. Res. Express. 3 (2016) 105023, https://doi.org/10.1088/2053-1591/3/10/105023.
[58] G. Wang, B. Huang, Z. Li, Z. Lou, Z. Wang, Y. Dai, M.-H. Whangbo, Synthesis and characterization of ZnS with controlled amount of S vacancies for photocatalytic H_2 production under visible light, Sci. Rep. 5 (2015) 8544, https://doi.org/10.1038/srep08544.
[59] M. Morales-Luna, M.A. Arvizu, M. Pérez-González, S.A. Tomas, Effect of a CdSe Layer on the Thermo- and Photochromic Properties of MoO_3 Thin Films Deposited by Physical Vapor Deposition, J. Phys. Chem. 123 (2019) 17083–17091, https://doi.org/10.1016/j.cattod.2018.04.065.
[60] Y.S. Kim, C.H. Park, Rich variety of defects in ZnO via an attractive interaction between o vacancies and Zn interstitials: origin of n-type doping, Phys. Rev. Lett. 102 (2009) 1–4, https://doi.org/10.1103/PhysRevLett.102.086403.
[61] M. Ponce-Mosso, M. Pérez-González, P.E. García-Tinoco, H. Crotte-Ledesma, M. Morales Luna, S.A. Tomás, Enhanced photocatalytic activity of amorphous MoO_3 thin films deposited by RF reactive magnetron sputtering, Catal. Today 349 (2020) 150–158, https://doi.org/10.1016/j.cattod.2018.04.065.
[62] D.A. Granada-Ramírez, A. Pulzara-Mora, C.A. Pulzara-Mora, A. Pardo-Sierra, J. A. Cardona-Bedoya, M. Pérez-González, S.A. Tomás, S. Gallardo-Hernández, J. G. Mendoza-Álvarez, Study of the surface chemistry, surface morphology, optical, and structural properties of InGaN thin films deposited by RF magnetron sputtering, Appl. Surf. Sci. 586 (2022) 152795, https://doi.org/10.1016/j.apsusc.2022.152795.
[63] M. Valenti, D. Dolat, G. Biskos, A. Schmidt-Ott, W.A. Smith, Enhancement of the photoelectrochemical performance of $CuWO_4$ thin films for solar water splitting by plasmonic nanoparticle functionalization, J. Phys. Chem. C 119 (2015) 2096–2104, https://doi.org/10.1021/jp506349t.
[64] M.A. Butler, Photoelectrolysis and physical properties of the semiconducting electrode WO_2, J. Appl. Phys. 48 (1977) 1914–1920, https://doi.org/10.1063/1.323948.
[65] M.A. Butler, D.S. Ginley, Prediction of flatband potentials at semiconductor-electrolyte interfaces from atomic electronegativities, J. Electrochem. Soc. 125 (1978) 228–232, https://doi.org/10.1149/1.2131419.
[66] K.M. Lee, C.W. Lai, K.S. Ngai, J.C. Juan, Recent developments of zinc oxide based photocatalyst in water treatment technology: a review, Water Res. 88 (2016) 428–448, https://doi.org/10.1016/j.watres.2015.09.045.
[67] M.A. Gondal, M.A. Suliman, M.A. Dastageer, G.K. Chuah, C. Basheer, D. Yang, A. Suwaiyan, Visible light photocatalytic degradation of herbicide (atrazine) using surface plasmon resonance induced in mesoporous Ag-WO_3/SBA-15 composite, J. Mole. Catal. A Chem. 425 (2016) 208–216, https://doi.org/10.1016/j.molcata.2016.10.015.
[68] J. Li, S.K. Cushing, D. Chu, P. Zheng, J. Bright, C. Castle, A. Manivan- nan, N. Wu, Distinguishing surface effects of gold nanoparticles from plasmonic effect on photoelectrochemical water splitting by hematite, J. Mater. Res. 11 (2016) 1608–1615, https://doi.org/10.1557/jmr.2016.102.
[69] H.G. Oliveira, L.H. Ferreira, R. Bertazzoli, C. Longo, Remediation of 17-α-ethinylestradiol aqueous solution by photocatalysis and electrochemically-assisted photocatalysis using TiO_2 and TiO_2/WO_3 electrodes irradiated by a solar simulator, Water Res. 72 (2015) 305–314, https://doi.org/10.1016/j.watres.2014.08.042.
[70] Y.M. Hunge, M.A. Mahadik, A.V. Moholkar, C.H. Bhosale, Photoelectrocatalytic degradation of oxalic acid using WO_3 and stratified WO_3/TiO_2 photocatalysts under sunlight illumination, Ultrason. Sonochem. 35 (2017) 233–242, https://doi.org/10.1016/j.ultsonch.2016.09.024.
[71] K. Sornalingam, A. McDonagh, J.L. Zhou, Photodegradation of estrogenic endocrine disrupting steroidal hormones in aqueous systems: progress and future challenges, Sci. Total Environ. 550 (2016) 209–224, https://doi.org/10.1016/j.scitotenv.2016.01.086.
[72] P.B. Fayad, A. Zamyadi, R. Broseus, M. Prévost, S. Sauvé, Degradation of progestagens by oxidation with potassium permanganate in wastewater effluents, Chem. Cent. J. 7 (2013) 84, https://doi.org/10.1186/1752-153X-7-84.